The Geological Society of America
Special Paper 454
2009

Late Quaternary sediment-accumulation rates within the inner basins of the California Continental Borderland in support of geologic hazard evaluation

William R. Normark[†]
Mary McGann*
Ray W. Sliter
U.S. Geological Survey, MS 999, 345 Middlefield Road, Menlo Park, California 94025, USA

ABSTRACT

An evaluation of the geologic hazards of the inner California Borderland requires determination of the timing for faulting and mass-movement episodes during the Holocene. Our effort focused on basin slopes and turbidite systems on the basin floors for the area between Santa Barbara and San Diego, California. Dating condensed sections on slopes adjacent to fault zones provides better control on fault history where high-resolution, seismic-reflection data can be used to correlate sediment between the core site and the fault zones. This study reports and interprets 147 radiocarbon dates from 43 U.S. Geological Survey piston cores as well as 11 dates from Ocean Drilling Program Site 1015 on the floor of Santa Monica Basin. One hundred nineteen dates from 39 of the piston cores have not previously been published. Core locations were selected for hazard evaluation, but despite the nonuniform distribution of sample locations, the dates obtained for the late Quaternary deposits are useful for documenting changes in sediment-accumulation rates during the past 30 ka. Cores from basins receiving substantial sediment from rivers, i.e., Santa Monica Basin and the Gulf of Santa Catalina, show a decrease in sediment supply during the middle Holocene, but during the late Holocene after sea level had reached the current highstand condition, rates then increased partly in response to an increase in El Niño–Southern Oscillation events during the past 3.5 ka.

INTRODUCTION

Radiocarbon dating of sediment from piston cores taken in the inner basins of the California Borderland was a major component of an effort to determine displacement history along faults and to date submarine landslides during the Holocene. Figure 1A shows some of the major faults of the inner Borderland and the location of piston cores taken for this study. Multichannel seismic-reflection surveys were used to map the main structural features summarized in Section 4 of this volume (regional tectonic structure and earthquake and tsunami hazards). High-resolution, seismic-reflection profiles were needed to resolve the shallow stratigraphy and structure of the sedimentary sections in the area of faults and landslides. Figure 1B shows the tracklines for the

[†]Deceased.
*Corresponding author: mmcgann@usgs.gov.

Normark, W.R., McGann, M., and Sliter, R.W., 2009, Late Quaternary sediment-accumulation rates within the inner basins of the California Continental Borderland in support of geologic hazard evaluation, *in* Lee, H.J., and Normark, W.R., eds., Earth Science in the Urban Ocean: The Southern California Continental Borderland: Geological Society of America Special Paper 454, p. 117–139, doi: 10.1130/2009.2454(2.6). For permission to copy, contact editing@geosociety.org.

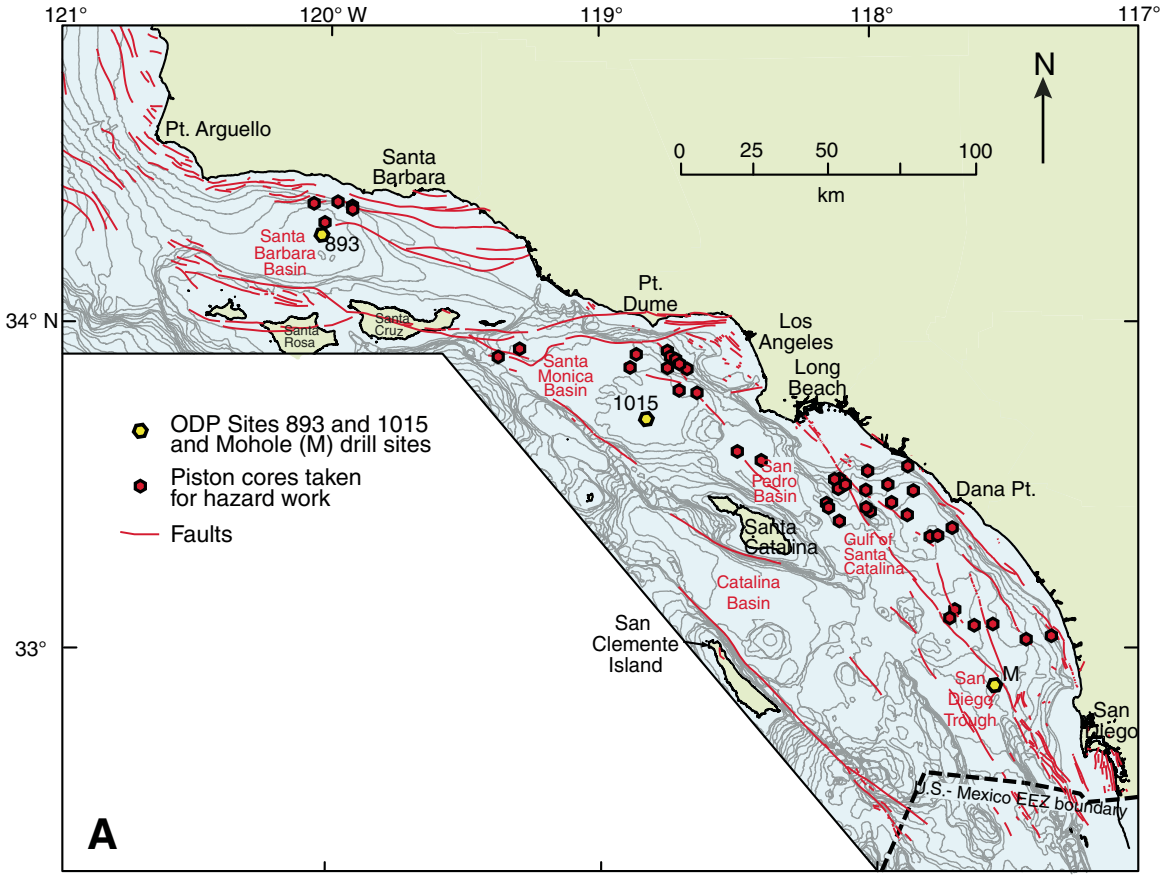

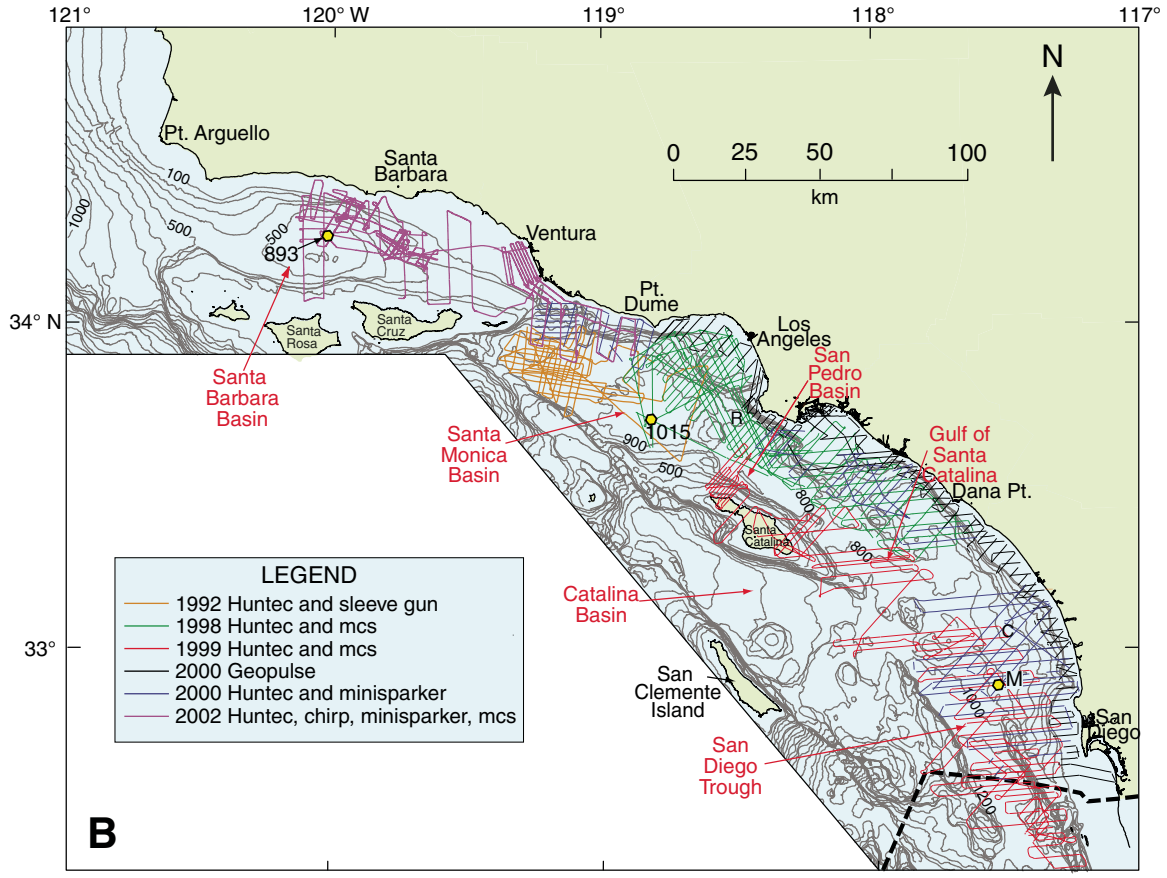

five major geophysical cruises that were used to obtain high-resolution reflection data using both surface and deep-towed boomer sources as well as a surface-towed chirp sonar system. The details of geophysical systems used are presented in Web-accessible U.S. Geological Survey (USGS) Open-File Reports (Normark et al., 1999a, 1999b; Gutmacher et al., 2000; Normark et al., 2003). In general, the boomer and chirp systems are capable of imaging reflectors with 0.5 m resolution; the deep-towed boomer system has the added advantage of deeper acoustic penetration for imaging sand-rich sediment deposits, and it is more effective for use in deep water.

The limited depth of penetration (generally <5 m) of piston cores in sedimentary sequences with interbedded silt and sand, which is common for inner Borderland basins, restricts direct sampling of most structures and landslides, e.g., offset surfaces along faults must lie within a few meters of the seafloor. Many core sites were chosen on basin slopes where both the rate of sedimentation and the grain sizes of the deposits are reduced compared to adjacent basin-floor settings; these "reduced sections" result in sampling older sediment than is possible adjacent to many active structures (see core distribution in Fig. 1A). The high-resolution reflection profiles are used to correlate a core site with a fault or landslide locality. Thus, samples from reduced sections provide the best chance to derive offset histories for active faults. Figure 2 shows the location of all cores that were taken in support of the offshore geologic hazard evaluation, and the schematic core logs show the depth of subsamples used for radiocarbon dating as well as the estimated depth to the base of the Holocene section at 11.6 ka (after Barron et al., 2003).

The results of the radiocarbon dating also provide an opportunity to reevaluate sediment-accumulation rates for the inner basins of the Borderland despite the nonuniform distribution of the samples (resulting from site selection in support of hazard evaluation). This chapter discusses the implications of changes in sediment-accumulation rates on basin floors and landward basin slopes during the past 30 ka (see preceding chapters in this volume for shelf and upper slope sedimentation histories).

Figure 1. (A) Map showing study area from Point Arguello to San Diego including the Borderland physiography, core locations used for this study, and the major offshore faults, which were the basis for selection of many of the core sites; fault pattern adapted from Fisher et al. (Chapter 4.4) and Ryan et al., this volume. Bathymetry simplified from National Oceanic and Atmospheric Administration (1998). (B) Map of the study area showing the tracklines for seismic-reflection data collected for the earthquake hazard task of the CABRILLO project. Terminology used in the legend refers to the types of seismic-reflection systems used: Huntec—high-resolution, deep-towed boomer source and receiver; Geopulse—high-resolution, surface-towed boomer source and receiver; minisparker and chirp—high-resolution, surface-towed sources and receivers; sleeve gun, source for single-channel profiles; mcs—multichannel seismic-reflection system using air-gun sources.

METHODS

Sampling History

The distribution of core sites reflects the availability of ship time, which was tied to other program sampling priorities in 1998, 1999, and 2003, the results of which are discussed elsewhere in this volume. The cores collected for hazard evaluation in 1998 are limited to the basin slope between Santa Monica Bay and deep Santa Monica Basin (Fig. 2). Seventeen radiometric dates from these cores as well as 11 dates from Ocean Drilling Program (ODP) Site 1015 on the basin floor are presented in Normark and McGann (2004). The dates from the 1998 cores are incorporated in this review, i.e., core Sites 361–366 (Fig. 2).

The first samples from the Gulf of Santa Catalina and San Diego Trough are from 1999, i.e., core Sites 501–511 (Fig. 2). Based on the preliminary results from the 1998 and 1999 cores, a final sampling cruise in 2003 attempted to address the remaining hazard issues. During the 2003 cruise, samples were obtained from all basins of the inner California Borderland north of the Exclusive Economic Zone (EEZ) boundary with Mexico. Information on all of these sampling cruises is available from: http://walrus.wr.usgs.gov/infobank/. The core stations for the 2003 cruise include the series 601–605, 645, 646, and 4329 and all cores with a letter and number identification, e.g., SMB2 (Fig. 2).

The USGS piston cores were logged for geotechnical properties (gamma-ray bulk density, sound velocity, and magnetic susceptibility), split, photographed, and a basic sedimentologic description completed to improve selection of sample intervals for radiocarbon dating. Figure 2 schematically shows all of the cores obtained; the horizontal solid green symbol in each core bar indicates the depth at which subsamples were selected for radiocarbon dating. The radiometric age data for these cores are presented in Tables 1–6. The range of ages for samples from the first two sampling cruises resulted in an inefficient selection of subsamples from some cores. As a result, for the 2003 cores, core-catcher samples were used when available to obtain the age at the bottom of the core. Additional samples were then selected from some cores to better define the age of fault offsets or submarine slide deposits as well as to better understand sediment-accumulation rate changes during the late Holocene.

Radiocarbon Dating

One hundred nineteen sediment samples from 39 new USGS cores were dated by accelerator mass spectrometry (AMS) ^{14}C using foraminifera and, in a few cases, mollusks (Tables 1–6). The tables give both reservoir-corrected and calibrated ages, but only calibrated ages are used to determine sediment-accumulation rates. Initially, we used monospecific, planktic foraminiferal samples of *Neogloboquadrina pachyderma* for age dating the samples. Later, we determined that the highest degree of precision possible by AMS dating was not necessary to answer the questions posed in this geologic hazard study, so the most abundant

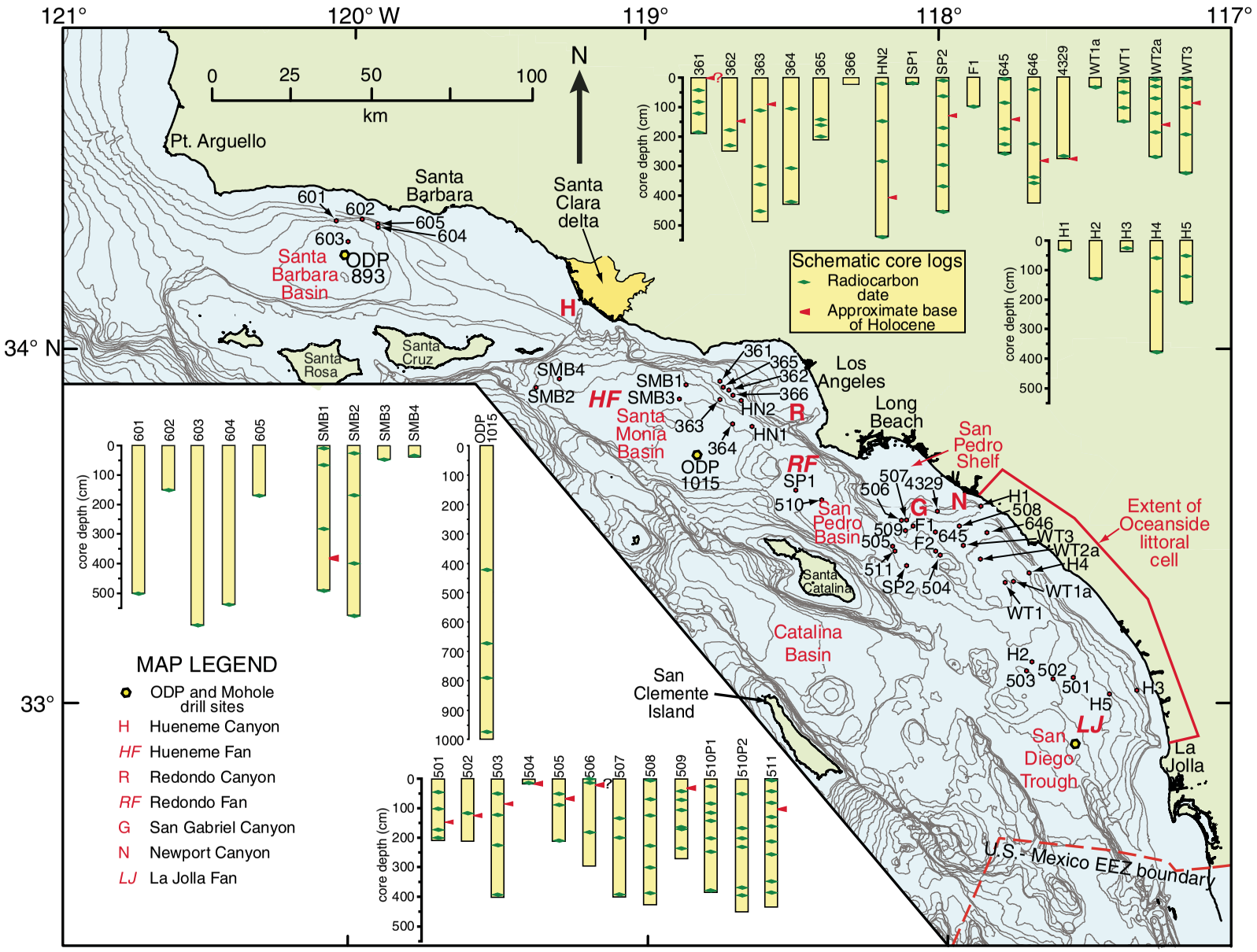

Figure 2. Map showing piston-core locations with their number designation (red dots with black rim) for the area in Figure 1 from Santa Barbara Basin to San Diego along with bathymetry (National Oceanic and Atmospheric Administration, 1998). Schematic representations of the cores show the Pleistocene–Holocene boundary (solid red triangle) in calibrated radiocarbon years and the depths at which samples were radiocarbon dated (flat green diamonds in the core depictions); where the green diamond appears below the core schematic, the date is from the core catcher sample (refer to Tables 1–6).

TABLE 1. RADIOCARBON DATES FOR CORES FROM SANTA BARBARA BASIN

NOSAMS* accession no.	Submitter identification	Meters below seafloor	Description	$\delta^{13}C$	Age	Age error	Age reservoir corrected	Calibrated age (yr B.P.)	Calibrated age error (yr B.P.)
OS-42042	A-1-03-SC **601-P1**, CC, 0–10 cm?	4.99–5.09	*Uvigerina* sp.	–0.83	8210	±50	6460	7375	±49
OS-42043	A-1-03-SC **602-G1**, CC, 0–10 cm?	1.50–1.60	Mixed benthic foraminifera	–1.09	3720	±40	1970	1996	±60
OS-41901	A-1-03-SC **603-P1**, CC, 0–10 cm?	6.06–6.16	Mixed benthic foraminifera	–1.08	4960	±40	3210	3506	±56
OS-42044	A-1-03-SC **604-P1**, CC, 0–10 cm?	5.36–5.46	*Uvigerina peregrina*	–0.83	4630	±35	2880	3121	±63
OS-41956	A-1-03-SC **605-G1**, CC, 0–12 cm	1.69–1.81	Mixed planktic foraminifera	0.07	3140	±30	2340	2442	±65

*NOSAMS—National Ocean Sciences accelerator mass spectrometry.

TABLE 2. RADIOCARBON DATES FOR CORES FROM SANTA MONICA BASIN

NOSAMS* accession no.	Submitter identification	Meters below seafloor	Description	$\delta^{13}C$	Age	Age error	Age reservoir corrected	Calibrated age (yr B.P.)	Calibrated age error (yr B.P.)
OS-55525	A-1-03-SC **SMB1-P1**, sec. 1, 8–10 cm	0.08–0.10	Mixed benthic foraminifera	–0.94	1770	±30	20		
OS-46159	A-1-03-SC **SMB1-P1**, sec. 2 , 30–32 cm	0.65–0.67	Mixed benthic foraminifera	–0.69	3010	±35	1260	1223	±39
OS-46160	A-1-03-SC **SMB1-P1**, sec. 3, 98–100 cm	2.83–2.85	Mixed benthic foraminifera	–1.07	9120	±50	7370	8243	±58
OS-42045	A-1-03-SC **SMB1-P1**, CC, 0–10 cm?	4.88–4.98	*Cassidulina tumida*	–1.99	12,900	±75	11,150	13,047	±75
OS-55526	A-1-03-SC **SMB2-P1**, sec. 1, 28–30 cm	0.28–0.30	Mixed benthic foraminifera	–1.98	2200	±30	450	481	±23
OS-46161	A-1-03-SC **SMB2-P1**, sec. 2, 32–34 cm	1.69–1.71	Mixed benthic foraminifera	–0.68	4160	±30	2410	2569	±58
OS-46162	A-1-03-SC **SMB2-P1**, sec. 3, 112–114 cm	3.99–4.01	Mixed benthic foraminifera	–1.04	7730	±50	5980	6853	±68
OS-41964	A-1-03-SC **SMB2-P1**, CC, 0–12 cm	5.72–5.84	Mixed benthic foraminifera	–1.60	8580	±40	6830	7693	±49
OS-42046	A-1-03-SC **SMB3-P1**, CC, 0–10 cm?	0.46–0.56	*Uvigerina* spp.	–0.22	3200	±30	1450	1388	±47
OS-42047	A-1-03-SC **SMB4-PG1**, 36–39 cm	0.36–0.39	Mixed benthic foraminifera	–0.67	2150	±30	400	446	±30
OS-46939	A-1-03-SC **HN1-P1**, CC, 0–10 cm	2.12–2.22	Mixed benthic foraminifera	–6.71	12,800	±55	11,050	12,970	±59
OS-55524	A-1-03-SC **HN2-P1**, sec. 1, 20–22 cm	0.20–0.22	Mixed benthic foraminifera	–0.94	1890	±30	140	179	±53
OS-47151	A-1-03-SC **HN2-P1**, sec. F, 70–72 cm	1.47–1.49	Mixed benthic foraminifera	–1.12	5850	±55	4100	4695	±83
OS-47160	A-1-03-SC **HN2-P1**, sec. D, 53–55 cm	2.82–2.84	Mixed benthic foraminifera	–1.25	9010	±50	7260	8117	±64
OS-42048	A-1-03-SC **HN2-P1**, CC, 0–11 cm	5.37–5.48	*Uvigerina* spp.	–1.33	13,000	±60	11,250	13,145	±55

*NOSAMS—National Ocean Sciences accelerator mass spectrometry.

TABLE 3. RADIOCARBON DATES FOR CORES FROM SAN PEDRO BASIN

NOSAMS* accession no.	Submitter identification	Meters below seafloor	Description	$\delta^{13}C$	Age	Age error	Age reservoir corrected	Calibrated age (yr B.P.)	Calibrated age error (yr B.P.)
OS-39143	O2-99-SC **505P1**, sec. 1, 50–52 cm	0.50–0.52	Mixed benthic foraminifera	0.16	9240	±35	7490	8357	±33
OS-31361	O2-99-SC **505P1**, sec. 1, 90–92 cm	0.90–0.92	*Neogloboquadrina pachyderma*	–0.7	13,550	±75	12,450	14,504	±218
OS-31447	O2-99-SC **505P1**, sec. 2, 113–115 cm	2.10–2.12	*Neogloboquadrina pachyderma*	–0.62	14,350	±75	13,250	15,696	±196
OS-36190	O2-99-SC **510P1**, sec. 1, 24–26 cm	0.24–0.26	*Neogloboquadrina pachyderma*	0.5	2020	±30	1220	1189	±42
OS-35631	O2-99-SC **510P1**, sec. 1, 83–85 cm	0.83–0.85	Mixed planktic foraminifera	1.45	4140	±35	3340	3667	±58
OS-31470	O2-99-SC **510P1**, sec. 1, 115–117 cm	1.15–1.17	*Neogloboquadrina pachyderma*	0.5	5180	±45	4380	5049	±91
OS-35632	O2-99-SC **510P1**, sec. 1, 143–145 cm	1.43–1.45	*Neogloboquadrina pachyderma*	1	6230	±45	5430	6249	±44
OS-36195	O2-99-SC **510P1**, sec. 2, 50–52 cm	2.00–2.02	*Neogloboquadrina pachyderma*	0.31	8320	±40	7520	8382	±39
OS-31471	O2-99-SC **510P1**, sec. 2, 94–96 cm	2.44–2.46	*Neogloboquadrina pachyderma*	0.12	8870	±55	8070	9093	±78
OS-31472	O2-99-SC **510P1**, sec. 3, 77–79 cm	3.77–3.79	*Neogloboquadrina pachyderma*	0.34	9850	±55	9050	10,303	±70
OS-35633	O2-99-SC **510P2**, sec. 1, 50–52 cm	0.50–0.52	*Neogloboquadrina pachyderma*	0.45	2030	±40	1230	1195	±47
OS-31473	O2-99-SC **510P2**, sec. 2, 18–20 cm	1.68–1.70	*Neogloboquadrina pachyderma*	0.52	4910	±80	4110	4696	±104
OS-35634	O2-99-SC **510P2**, sec. 2, 50–52 cm	2.00–.202	*Neogloboquadrina pachyderma*	0.59	6270	±45	5470	6289	±52
OS-35635	O2-99-SC **510P2**, sec. 2, 80–82 cm	2.30–2.32	*Neogloboquadrina pachyderma*	0.18	6870	±45	6070	6969	±71
OS-35636	O2-99-SC **510P2**, sec. 3, 68–70 cm	3.68–3.70	*Neogloboquadrina pachyderma*	0.25	9000	±50	8200	9265	±84
OS-31474	O2-99-SC **510P2**, sec. 3, 95–97 cm	3.95–3.97	*Neogloboquadrina pachyderma*	0.22	9210	±70	8410	9475	±58
OS-42049	A-1-03-SC **SP1-P1**, CC, 0–10 cm	0.22–0.32	*Uvigerina peregrina dirupta*	–0.33	2360	±30	610	590	±34

*NOSAMS—National Ocean Sciences accelerator mass spectrometry.

foraminiferal species in each sample were utilized instead. As a result, nine radiocarbon dates were determined using the benthic genus *Uvigerina (U. peregrina*, *U. peregrina dirupta, U. juncea,* or mixtures of the first two species), seven samples with the benthic genera *Cassidulina*, *Cibicides*, or *Gyroidina*, and 68 samples using a mixed benthic foraminiferal assemblage. Thirty-one samples used planktic foraminifera, including 23 with *Neogloboquadrina pachyderma* and another eight with a mixed planktic foraminiferal assemblage (mostly *N. pachyderma, N. dutertrei, and Globigerina bulloides*). In addition, four mollusks were dated, including three bivalves and one gastropod.

Radiocarbon ages were also obtained for 11 samples from ODP Hole 1015B in Santa Monica Basin (Normark and McGann, 2004). This core is important because it provides a good record of total sediment input since oxygen isotope stage 3 (Martinson et al., 1987) in this closed basin, thereby providing a good comparison to the open basins to the south. Foraminifera were used to date these samples as well. One of these was determined using the planktic foraminifer *N. pachyderma*; the remainder used benthic foraminifera, including five samples with the genus *Uvigerina*, and five of a mixed benthic assemblage (Normark and McGann, 2004).

Radiocarbon dating was provided by the National Ocean Sciences AMS (NOSAMS) Facility at the Woods Hole Oceanographic Institution. Ages were calculated using the accepted half-life of ^{14}C of 5568 yr (Stuiver and Polach, 1977). The original measurements were obtained by a $^{14}C/^{12}C$ ratio and corrected for isotope fractionation by normalizing for $\delta^{13}C$ by NOSAMS. Raw radiocarbon ages between 0 and ca. 22 ka were then converted to calibrated ages using the CALIB 5.0.1 program (Stuiver and Reimer, 1993), and those between ca. 22 and 50 ka were converted to calibrated ages using the timescale proposed by Shackleton et al. (2004) based on paired ^{230}Th and ^{14}C measurements on pristine corals. A reservoir age of 1750 yr was chosen for the benthic foraminiferal samples following Mix et al. (1999), and similarly applied to the mollusks because they occupied the same substrate as the benthic foraminifera. An 800 yr reservoir age was used for the planktic foraminiferal samples with radiocarbon ages younger than 12,000 yr (Southon et al., 1990; Kienast and McKay, 2001), and an 1100 yr reservoir age for those older than 12,100 yr (Kovanen and Easterbrook, 2002).

RADIOMETRIC DATES AND APPLICATION TO HAZARD EVALUATION

This section gives the geographic setting for the piston-core stations and a brief statement of the rationale for selecting the core sites. The core sites are grouped by basin or by tectonic objective. Examples of how the radiometric age data are used to ascertain timing of fault movements and submarine landslides are included but are not the main topic for this chapter, which is to use the data to provide insight regarding sediment-accumulation rates during the late Quaternary. The structure and tectonic setting are covered in Section 4 of this volume.

TABLE 4. RADIOCARBON DATES FOR CORES ADJACENT TO THE PALOS VERDES FAULT

NOSAMS* accession no.	Submitter identification	Meters below seafloor	Description	$\delta^{13}C$	Age	Age error	Age reservoir corrected	Calibrated age (yr B.P.)	Calibrated age error (yr B.P.)
OS-39142	O2-99-SC **504P1**, sec. 1, 13–15 cm	0	Mixed benthic foraminifera	0.23	11,600	±45	9,850	11,225	±37
OS-40074	O2-99-SC **506P1**, Sec. 1, 0–2 cm	0.00–0.02	Mixed benthic foraminifera	–0.29	2270	±35	520	524	±28
OS-31448	O2-99-SC **506P1**, sec. 1, 14–16 cm	0.14–0.16	*Neogloboquadrina pachyderma*	0.38	10,100	±60	9,300	10,559	±55
OS-36193	O2-99-SC **506P1**, sec. 1, 14–16 cm	0.14–0.16	Mollusk	1.86	10,850	±40	9,100	10,352	±68
OS-39144	O2-99-SC **506P1**, sec. 3, 35–37 cm	1.82–1.84	Mixed benthic foraminifera	–1.93	36,800	±270	35,050	42,500	
OS-39145	O2-99-SC **507P1**, sec. 2, 20–22 cm	1.35–1.37	Mixed benthic foraminifera	–0.75	21,800	±80	20,050	24,011	±136
OS-39146	O2-99-SC **507P1**, sec. 2, 83–85 cm	1.98–2.00	Mixed benthic foraminifera	–1.02	47,800	±1400	46,050	48,200	
OS-31449	O2-99-SC **507P1**, sec. 4, 78–80 cm	3.90–3.92	*Neogloboquadrina pachyderma*	–3.29	44,400	±870	43,300	47,500	
OS-36194	O2-99-SC **509P1**, sec. 1, 41–42 cm	0.41–0.42	Mollusk	1.63	13,300	±60	11,550	13,380	±63
OS-39179	O2-99-SC **509P1**, sec. 1, 70–72 cm	0.70–0.72	Mixed benthic foraminifera	0.1	15,000	±60	13,250	15,695	±185
OS-39180	O2-99-SC **509P1**, sec. 1, 105–107 cm	1.05–1.07	Mixed benthic foraminifera	–0.09	17,150	±75	15,400	18,749	±64
OS-31468	O2-99-SC **509P1**, sec. 2, ~15 cm	1.65±	gastropod	–0.03	31,300	±400	29,550	36,700	
OS-39181	O2-99-SC **509P1**, sec. 2, 20–22 cm	1.70–1.72	Mixed benthic foraminifera	–0.3	32,200	±200	30,450	37,700	
OS-31469	O2-99-SC **509P1**, sec. 2, 85–87 cm	2.35–2.37	Mixed planktic foraminifera	–0.34	38,800	±680	37,700	44,200	
OS-55521	O2-99-SC **511P1**, sec. 1, 2–4 cm	0.02–0.04	Mixed benthic foraminifera	–0.61	2070	±30	320	364	±44
OS-39182	O2-99-SC **511P1**, sec. 1, 40–42 cm	0.40–0.42	Mixed planktic foraminifera	1.05	3890	±35	3,090	3,374	±42
OS-39183	O2-99-SC **511P1**, sec. 1, 80–82 cm	0.80–0.82	Mixed planktic foraminifera	0.73	8560	±40	7,760	8,643	±67
OS-31475	O2-99-SC **511P1**, sec. 2, 19–21 cm	1.29–1.31	*Neogloboquadrina pachyderma*	0.44	12,600	±80	11,500	13,343	±72
OS-55522	O2-99-SC **511P1**, sec. 2, 50–52 cm	1.60–1.62	Mixed benthic foraminifera	–0.26	21,800	±140	20,050	24,006	±186
OS-55523	O2-99-SC **511P1**, sec. 3, 20–22 cm	2.10–2.12	Mixed benthic foraminifera	–0.5	30,800	±280	29,050	36,600	
OS-39184	O2-99-SC **511P1**, sec. 3, 65–67 cm	2.55–2.57	*Uvigerina peregina*	–0.87	35,000	±280	33,250	40,600	
OS-39185	O2-99-SC **511P1**, sec. 4, 8–10 cm	3.48–3.50	*Neogloboquadrina pachyderma*	0.28	43,100	±600	42,000	46,900	
OS-39186	O2-99-SC **511P1**, sec. 4, 44–46 cm	3.84–3.86	Mixed planktic foraminifera	0	51,700	±1500	50,600		
OS-41957	A-1-03-SC **F1-P1**, CC, 0–7 cm	0.89–0.96	*Cibicides* sp.	–0.02	34,500	±730	32,750	40,000	
OS-41958	A-1-03-SC **F2-P1**, CC, 0–7 cm	0.00–0.07	*Cassidulina* spp.	–0.04	21,800	±150	20,050	24,006	±196

*NOSAMS—National Ocean Sciences accelerator mass spectrometry.

TABLE 5. RADIOCARBON DATES FOR CORES THE GULF OF SANTA CATALINA

NOSAMS* accession no.	Submitter identification	Meters below seafloor	Description	$\delta^{13}C$	Age	Age error	Age reservoir corrected	Calibrated age (yr B.P.)	Calibrated age error (yr B.P.)
OS-55519	O2-99-SC **508P1**, sec 1, 3–5 cm	0.03–0.05	Mixed planktic foraminifera	–0.58	1060	±25	(–690)		
OS-35617	O2-99-SC **508P1**, sec 1, 70–72 cm	0.70–0.72	Mixed planktic foraminifera	1.17	2530	±30	1,730	1720	±50
OS-40075	O2-99-SC **508P1**, Sec. 1, 125–127 cm	1.25–1.27	Mixed benthic foraminifera	–0.52	4300	±35	2550	2729	±29
OS-39147	O2-99-SC **508P1**, sec. 2, 100–102 cm	2.28–2.30	Mixed benthic foraminifera	0.65	6560	±40	4810	5574	±47
OS-55520	O2-99-SC **508P1**, sec. 3, 24–26 cm	3.00–3.02	Mixed benthic foraminifera	–0.62	8420	±60	6670	7551	±56
OS-31450	O2-99-SC **508P1**, sec. 3, 110–112 cm	3.86–3.88	*Neogloboquadrina pachyderma*	0.38	9320	±60	8520	9584	±72
OS-55641	A-1-03-SC **SP2-P1**, sec. D, 10–12 cm	0.10–0.12	Mixed benthic foraminifera	–0.63	3960	±35	2210	2295	±46
OS-46077	A-1-03-SC **SP2-P1**, sec. C, 45–47 cm	0.63–0.65	Mixed benthic foraminifera	–0.88	10,100	±80	8350	9418	±80
OS-46078	A-1-03-SC **SP2-P1**, sec. B, 1.5–3.5 cm	1.695–1.715	Mixed benthic foraminifera	–1.36	12,050	±50	10,300	12,074	±82
OS-55640	A-1-03-SC **SP2-P1**, sec. B, 60–62 cm	2.28–2.30	Mixed benthic foraminifera	–1.38	15,550	±60	13,800	16,434	±203
OS-46079	A-1-03-SC **SP2-P1**, sec. B, 127–129 cm	2.95–2.97	*Cibicides* sp.	–1.29	20,400	±100	18,650	22,228	±94
OS-46076	A-1-03-SC **SP2-P1**, sec. A, 67–69 cm	3.68–3.70	*Cibicides* sp.	–0.26	24,400	±150	22,650	28,500	
OS- 41965	A-1-03-SC **SP2-P1**, CC, 0–14 cm	4.51–4.65	Mixed benthic foraminifera	–1.56	23,400	±200	21,650	27,300	
OS-55642	A-1-03-SC **WT1-P1**, sec. 1, 10–12 cm	0.10–0.12	Mixed benthic foraminifera	–0.85	2010	±30	260	305	±35
OS-47091	A-1-03-SC **WT1-P1**, sec. 1, 50–52 cm	0.50–0.52	Mixed benthic foraminifera	–0.78	4390	±40	2640	2807	±46
OS-47092	A-1-03-SC **WT1-P1**, sec. 1, 100–102 cm	1.00–1.02	Mixed benthic foraminifera	–0.90	8010	±50	6260	7194	±51
OS-42038	A-1-03-SC **WT1-P1**, Sec 2, 44.5–45.5	1.48–1.49	Mixed benthic foraminifera	–1.47	10,450	±50	8700	9841	±109
OS-42039	A-1-03-SC **WT1A-P1**, CC, 0–10 cm?	0.30–0.40	Mixed benthic foraminifera	–0.89	2460	±35	710	667	±29
OS-55643	A-1-03-SC **WT2A-P1**, sec. 1, 4–6 cm	0.04–0.06	Mixed benthic foraminifera	–0.67	1910	±35	160	194	±12
OS-55644	A-1-03-SC **WT2A-P1**, sec. 1, 30–32 cm	0.30–0.32	Mixed benthic foraminifera	–0.7	4250	±30	2,500	2692	±33
OS-46163	A-1-03-SC **WT2A-P1**, sec. 1, 70–72 cm	0.70–0.72	Mixed benthic foraminifera	–0.92	8930	±50	7180	8041	±63
OS-46164	A-1-03-SC **WT2A-P1**, sec. 2, 4–6 cm	1.20–1.22	Mixed benthic foraminifera	–1.14	10,800	±40	9050	10,297	±59
OS-47093	A-1-03-SC **WT2A-P1**, sec. 2, 70–73 cm	1.86–1.89	Mixed benthic foraminifera	–1.22	11,750	±60	10,000	11,472	±72
OS-42040	A-1-03-SC **WT2A-P1**, CC, 0–12 cm	2.67–2.79	*Uvigerina juncea*	–1.42	13,550	±80	11,800	13,652	±99
OS-55645	A-1-03-SC **WT3-P1**, sec. 1, 6–8 cm	0.06–0.08	Mixed benthic foraminifera	–0.71	2900	±40	1150	1108	±54
OS-46165	A-1-03-SC **WT3-P1**, sec. 2, 10–12 cm	0.30–0.32	Mixed benthic foraminifera	–0.80	5130	±40	3380	3723	±65
OS-46074	A-1-03-SC **WT3-P1**, sec. 2, 81–83 cm	1.01–1.03	Mixed benthic foraminifera	–1.19	12,700	±65	10,950	12,897	±38
OS-46075	A-1-03-SC **WT3-P1**, sec. 3, 22–24 cm	1.93–1.95	Mixed benthic foraminifera	–2.17	13,950	±65	12,200	14,054	±80
OS-42041	A-1-03-SC **WT3-P1**, CC, 0–13 cm	3.21–3.34	*Gyroidina altiformis*	–1.43	14,700	±85	12,950	15,291	±162
OS-41959	A-1-03-SC **H1-P1**, CC, 0–8 cm	0.30–0.38	Mixed benthic foraminifera	–0.04	2740	±30	990	937	±33
OS-55535	A-1-03-SC **H4-P1**, sec. C, 60–62 cm	0.60–0.62	Mixed benthic foraminifera	–1.66	2800	±40	1050	996	±48
OS-55536	A-1-03-SC **H4-P1**, sec. B, 100–102 cm	1.73–1.75	Mixed benthic foraminifera	–1	5590	±40	3840	4344	±60
OS-41962	A-1-03-SC **H4-P1**, CC, 0–10 cm?	3.74–3.84	Mixed benthic foraminifera	–2.35	10,950	±65	9200	10,460	±73
OS-55646	A1-03-SC **645-P1,** sec. 1, 4–6 cm	0.04–0.06	Mixed benthic foraminifera	–0.51	1120	±30	(–630)		
OS-55853	A1-03-SC **645-P1,** sec. 1, 85–87 cm	0.85–0.87	Mixed benthic foraminifera	0	10,100	±50	8350	9419	±49
OS-55604	A1-03-SC **645-P1,** sec. 2, 70–72 cm	1.74–1.76	Mixed benthic foraminifera	–0.81	12,700	±65	10,950	12,897	±38
OS-46934	A1-03-SC **645-P1**, sec. 2, 120–122 cm	2.24–2.26	Mixed benthic foraminifera	–1.37	13,600	±65	11,850	13,711	±71
OS-46935	A1-03-SC **645-P1**, CC	2.54–2.60	Mixed benthic foraminifera	–0.29	9420	±40	7670	8526	±54
OS-55607	A1-03-SC 646-P1, sec. 1, 40–42 cm	0.40–0.42	Mixed benthic foraminifera	–0.68	3410	±35	1660	1631	±53
OS-55608	A1-03-SC 646-P1, sec. 2, 98–100 cm	2.25–2.27	Mixed benthic foraminifera	–1.09	10,150	±50	8400	9469	±40
OS-46936	A1-03-SC **646-P1**, sec. 3, 60–62 cm	3.37–3.39	*Uvigerina peregrina*	–1.08	12,700	±60	10,950	12,896	±35
OS-46937	A1-03-SC **646-P1**, sec. 3, 79–81 cm	3.56–3.58	*Uvigerina peregrina*	–1.15	12,900	±50	11,150	13,046	±60
OS-46938	A1-03-SC **4329-P1**, sec. A, 143–145 cm	2.69–2.71	Mixed benthic foraminifera	–0.39	11,000	±45	9250	10,518	±41

*NOSAMS—National Ocean Sciences accelerator mass spectrometry.

TABLE 6. RADIOCARBON DATES FOR CORES FROM SAN DIEGO TROUGH

NOSAMS* accession no.	Submitter identification	Meters below seafloor	Description	$\delta^{13}C$	Age	Age error	Age reservoir corrected	Calibrated age (yr B.P.)	Calibrated age error (yr B.P.)
OS-39102	O2-99-SC **501P1**, sec. 1, 45–47 cm	0.45–0.47	Mixed benthic foraminifera	1.13	5760	±40	4010	4570	±73
OS-36192	O2-99-SC **501P1**, sec. 1, 100–102 cm	1.00–1.02	Mollusk	1.45	5610	±30	3860	4372	±50
OS-40073	O2-99-SC **501P1**, sec. 2, 21–23 cm	1.71–1.73	Mixed benthic foraminifera	–1.34	14,200	±70	12,450	14,502	±213
OS-31357	O2-99-SC **501P1**, sec. 2, 49–51 cm	1.99–2.01	*Neogloboquadrina pachyderma*	–0.1	14,250	±80	13,150	15,554	±190
OS-31358	O2-99-SC **502P1**, sec. 1, 118–120 cm	1.18–1.20	*Neogloboquadrina pachyderma*	0.42	9820	±55	9020	10,270	±68
OS-39139	O2-99-SC **503P1**, sec. 1, 50–52 cm	0.50–0.52	Mixed benthic foraminifera	1.76	8280	±30	6530	7441	±29
OS-39140	O2-99-SC **503P1**, sec. 3, 10–12 cm	1.22–1.24	Mixed benthic foraminifera	–0.13	15,100	±60	13,350	15,843	±189
OS-31359	O2-99-SC **503P1**, sec. 3, 112–114 cm	2.24–2.26	*Neogloboquadrina pachyderma*	0	37,000	±300	35,900	42,600	
OS-31360	O2-99-SC **503P1**, sec. 4, 131–135 cm	3.91–3.95	*Neogloboquadrina pachyderma*	–0.37	40,300	±1000	39,200	45,200	
OS-41960	A-1-03-SC **H2-P1**, CC, 0–10 cm?	1.26–1.36	Mixed benthic foraminifera	–0.85	10,700	±55	8950	10,196	±50
OS-41961	A-1-03-SC **H3-P1**, CC, 0–14 cm	0.16–0.30	*Cassidulina* sp.	0.66	7470	±35	5720	6551	±54
OS-55528	A-1-03-SC **H5-P1**, sec. B, 50–52 cm	0.50–0.52	Mixed benthic foraminifera	–0.14	18,950	±100	17,200	20,318	±130
OS-55527	A-1-03-SC **H5-P1**, sec. A, 64–66 cm	1.22–1.24	Mixed benthic foraminifera	–0.63	48,600	±1400	46,850	48,000	
OS-41963	A-1-03-SC **H5-P1**, CC, 0–10 cm	2.08–2.18	Mixed benthic foraminifera	–0.75	27,500	±270	25,750	31,300	

*NOSAMS—National Ocean Sciences accelerator mass spectrometry.

Basin Setting and Sampling Strategy

Santa Barbara Basin

The radiometric age data are presented from west to east, beginning with Santa Barbara Basin. The late Pleistocene depositional history of the basin floor of Santa Barbara Basin is well known from extensive study of cores recovered at ODP Site 893 (Fig. 2; Shorebased Scientific Party, 1994; Kennett and Venz, 1995; Behl and Kennett, 1996). Much of the basin fill from the past 500 ka is silty mud, which is massive, if deposited during periods when the bottom waters are oxygenated (and bioturbated) but is laminated during anoxic conditions (Behl et al., 2005; Kennett et al., 2005). These studies also confirm that unlike all other basins of the inner Borderland, Santa Barbara Basin has relatively minor coarser grained deposits resulting from turbidity-current processes. The USGS objectives for coring in this basin were focused on refining estimates of the age of large landslides offshore Goleta, California (Greene et al., 2004; Fisher et al., 2005; Lee et al., this volume). Five cores (Sites 601–605), which are from the slide scarp area and the surface of the slide debris, all only recovered Holocene sediment (Table 1) that postdates the youngest of the failure events identified by Fisher et al. (2005).

Santa Monica Basin

Sediment accumulation in Santa Monica Basin has been studied for nearly half a century with an emphasis on turbidity-current deposits (e.g., Gorsline and Emery, 1959; Nardin, 1983; Gorsline, 1996; Normark et al., 1998). ODP Site 1015 (Fig. 2) was drilled in the deepest part of the basin to provide a comparison with Site 893 in Santa Barbara Basin for paleoceanographic investigation, but the sand-rich turbidite sequence was deemed unsuitable for that purpose (Shipboard Scientific Party, 1997). Extensive piston and box coring in the Santa Monica Basin area both before and during the hazard assessment work helps provide the most complete picture of sediment-accumulation rates for any of the basins offshore Southern California (e.g., Reynolds, 1987; Christensen et al., 1994; Gorsline, 1996; Sommerfield and Lee, 2003, 2004; Normark and McGann, 2004; Alexander et al., this volume; Sommerfield et al., this volume). The dates presented here (Table 2) are for the deeper part of the basin on the Dume and Hueneme fan areas; the feeding canyons for both these turbidite systems cross major faults along the basin slope. The intent is to better understand the history of turbidite deposition during sea-level rise, thus building on the results of Piper et al. (1999) and Normark and McGann (2004). The initial results have been tied to a basinwide chronostratigraphy correlated to ODP Site 1015 and are discussed in the following chapter (Normark et al., this volume, Chapter 2.7).

San Pedro Basin

The San Pedro Basin is dominated by the Redondo Fan to the north and the Palos Verdes debris avalanche in the mid basin (Fig. 2; Fig. 8 in Normark et al., this volume, Chapter 2.7). The

Redondo Fan is a sand-rich deposit, and attempts to establish a Holocene depositional history for the fan were largely unsuccessful; the one core recovered from the middle fan was only 32 cm long, including the catcher sample (Table 3). The Palos Verdes debris avalanche moved into the basin from the adjacent slope area that forms the northern wall of the San Pedro sea valley, and avalanche movement was guided by the right-hand levee extending into the basin from the base of the slope. Two cores were taken at Site 510, a short distance from the toe of the main avalanche deposits, which carried blocks as tall as 20 m. The high-resolution boomer data showed that a sequence with an acoustic facies characteristic of well-bedded turbidite deposits underlies the avalanche deposits and provides a limit for the age of the mass failure deposit (Normark et al., 2004b). Dating of the Palos Verdes debris avalanche is reviewed later in this chapter.

The only other core from the San Pedro Basin area is from the lower slope near the southeastern end of the basin. Core Site 505 (Table 3) from the flank of a small, faulted bathymetric high was selected to obtain a condensed section.

Palos Verdes Fault System

Several cores were taken during the 1999 and 2003 sampling programs with the purpose of documenting the timing of movement on the Palos Verdes fault system (Figs. 1A and 2; Table 4). The core sites selected include attempts to date offset reflectors within tens of meters of a fault strand (Sites 507, F1, and F2) as well as condensed sections where the late Quaternary acoustic stratigraphy can be used to tie the site to the fault (Sites 506, 509, and 511). An example of each kind of target site is discussed below to illustrate the difficulties that can be encountered.

Gulf of Santa Catalina

The Gulf of Santa Catalina is a large area between the coast and Santa Catalina Island extending from the shelf off Long Beach to south of Dana Point, California (Fig. 1). Two major fault systems cut through the area: Palos Verdes in the western part and Newport-Inglewood along the eastern side (Ryan et al., this volume). Two submarine canyons, both with multiple tributaries, head along or near these faults where they cross the edge of the San Pedro Shelf and feed sediment to different parts of Gulf of Santa Catalina (Fig. 22 in Normark et al., this volume, Chapter 2.7). The San Gabriel Canyon enters adjacent to the Palos Verdes fault zone, and the Newport Canyon is along the eastern margin (see Fig. 1 in Chapter 2.7). Unlike the previously described basins, which are closed systems, the Gulf of Santa Catalina is an open basin, and much sediment is lost to other parts of the Borderland. Turbidity currents moving through the San Gabriel Canyon and channel system can reach Catalina Basin west of Santa Catalina Island (Fig. 2). The Newport channel system ultimately feeds sediment into San Diego Trough, which is the next basin south (see Chapter 2.7).

Piston-core sites from the Gulf of Santa Catalina were selected to provide age control for high-resolution stratigraphy and to document the change from turbidite sedimentation to hemipelagic facies in some areas as suggested by the deep-tow boomer data. In the high-resolution boomer records, locally thick, acoustically transparent sediment overlies units with high-amplitude bedded units typical of turbidite deposits. The schematic core representations of Figure 2 show that only about half of the cores from this area penetrated the entire Holocene section (Table 5); many of the cores are short because of the sandy nature of much of the area.

San Diego Trough

San Diego Trough is a linear, fault-bounded basin that receives sediment from the Newport Canyon as well as several submarine canyons along its eastern margin (Fig. 2; Fig. 22 in Normark et al., this volume, Chapter 2.7). Several major fault systems extend from the onshore San Diego and offshore San Diego Trough areas to merge with structures in the Gulf of Santa Catalina (see Ryan et al., this volume). The core sites were selected to date movement on parts of these faults and to date the cessation of turbidity-current deposition observed for small fans along the eastern margin of the Trough (Fig. 2 and Table 6). Similar to the Gulf of Santa Catalina, San Diego Trough is an open basin, with sediment moving into the EEZ of Mexico and from there to San Clemente Basin to the west (south of the EEZ boundary with Mexico; Fig. 2).

Timing of Submarine Fault and Slide Movements

The northeastern margin of Santa Monica Basin is bounded by fault and fold structures, some of which are young and occur in basin-floor turbidite sediment (see Fig. 16 in Fisher et al., 2003; Normark and Piper, 1998). A high-resolution stratigraphic framework for the basin fill has been tied to the dated sediment sequence cored at ODP Site 1015, thus providing age control for the framework (Normark and McGann, 2004). The dated horizons can be traced from the drill site to both ends of the basin and onto the lowermost slope in some areas. Offset or folding observed in these horizons might be able to give the timing of deformation without need for a core on, or adjacent to, the structure in question.

The stratigraphic framework tied to ODP Site 1015 can be extended onto the lowermost basin slopes along the less steep margins of the basin. Two cores were obtained at opposite ends of Santa Monica Basin to date the upper part of the stratigraphic framework to confirm the correlation with ODP Site 1015 (cores SMB2 and 364; see Figs. 2 and 3). Both piston cores were taken ~40 m above the adjacent basin floor, and in both cases the key horizons L to O could be extended from the basin floor to the core sites. At both ends of the basin, the interval between the key horizons thins as water depth decreases (Fig. 3). The cores also confirmed that the lower slope deposits include fine-grained, thin turbidite deposits, which are the key to the basinwide stratigraphy. This record of flow thickness at core 364 on the western basin slope is consistent with deposition on the western high levee of the Hueneme fan valley, which has ~40 m relief above

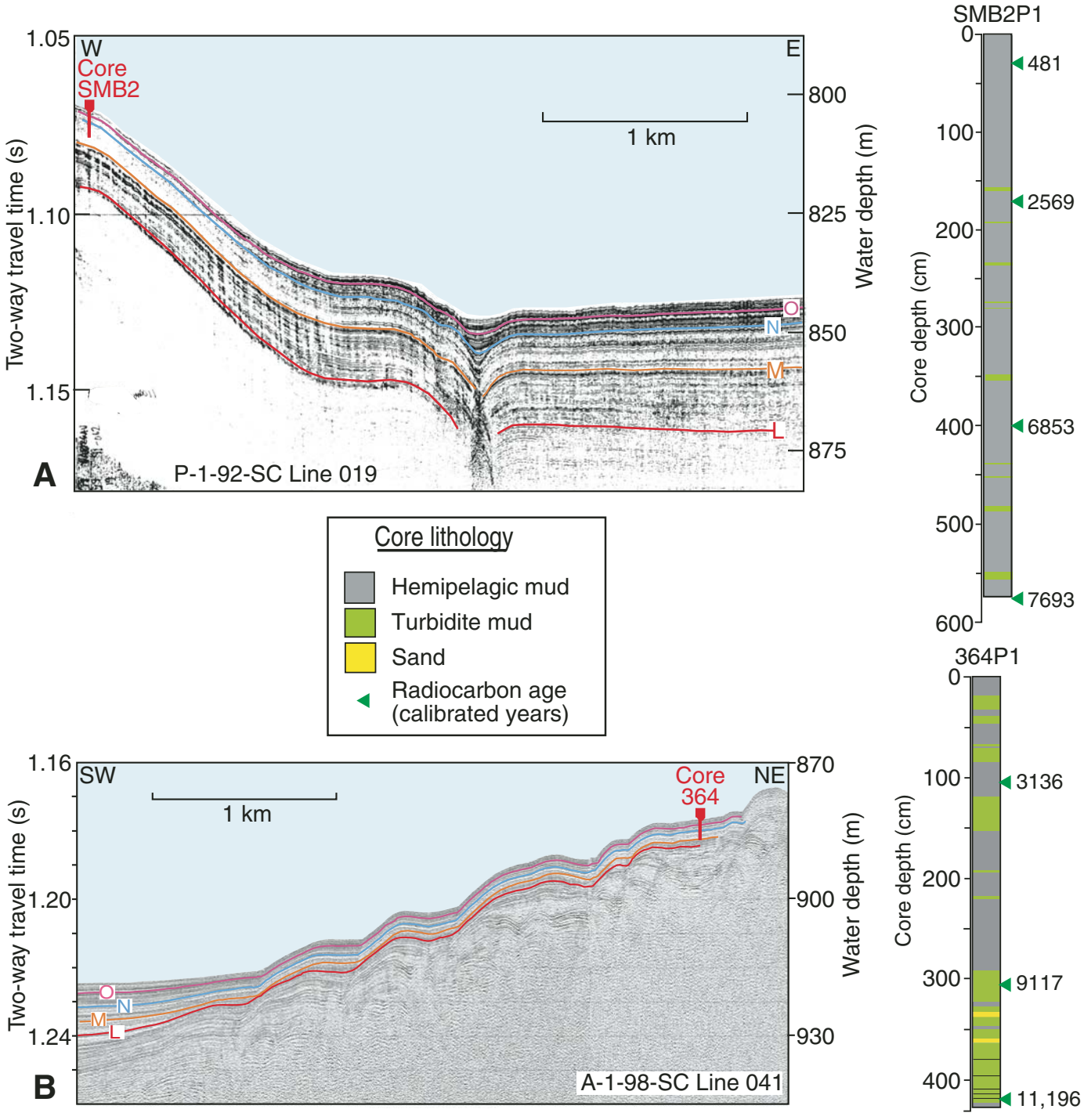

Figure 3. Deep-tow boomer profile segments from Santa Monica Basin comparing deposition on the lower basin slopes at opposite ends of the basin. Reflectors O to L are regional reflectors that are tentatively correlated through the deep-tow boomer profiles with Ocean Drilling Program (ODP) Site 1015 (Fig. 1B) and that can be mapped throughout much of Santa Monica Basin (Normark et al., 2006). Ages shown on the accompanying sediment logs are yr B.P. (see Table 2 for core SMB2P1 and Normark and McGann, 2004, for core 364P1).

the main channel floor (see Fig. 6 in Normark et al., this volume, Chapter 2.7). Thus, it appears that turbidity currents flowing from the Hueneme Canyon commonly exceed 40 m in thickness and that the flow thickness tends to be maintained to the distal (eastern) end of the basin.

It was initially thought that growth folding could be dated using the high-resolution stratigraphic framework, e.g., where fold structures show a thinning of the layers across the uplifting crestal area. Because turbidity currents are depositing sediment well above the basin floor, it becomes difficult to place timing constraints on growth folds on the basin floor. This is because turbidity currents transport a reduced amount of suspended sediment with increasing elevation within the current. Deposition on an existing high on the basin floor will therefore result in thinner beds across the crestal area simply as a result of deposition from turbidity currents with or without growth of the anticlinal relief.

Dating fault offsets and submarine slide emplacement is more straightforward using the detailed stratigraphic framework. For example, the depression in the middle of the deep-tow boomer profile of Figure 3A marks the surface expression of a strike-slip fault along the western margin of Santa Monica Basin. The uppermost key horizons O and N are seen to be continuous across the depression, and deposition during this interval results in a gradual reduction in relief. Based on the ages for the stratigraphic sequence at ODP Site 1015, reflector O is 1.65 ka, and N is 4.27 ka. These ages are in good agreement with the radiocarbon results for core SMB2, where reflector O is at ~120 cm depth and N is ~260 cm. The next deepest key reflector, M, is offset at the depression; M, which was not penetrated by core SMB2, is ca. 7.5 ka at ODP Site 1015 suggesting that the last fault movement at this site was slightly after 7 ka (Fig. 3A).

Where no ODP or equivalent drill hole is available, it is more difficult to establish a basinwide stratigraphic framework. The deep-tow boomer profiles of Figure 4 show the advantages of using cores from condensed sections to determine regional stratigraphy and hence offset histories. The profile shown in Figure 4B crosses a strand of the Coronado Bank–Palos Verdes fault zone; this strand is steeply dipping and bends slightly to trend more northerly than the main Palos Verdes fault zone (see Ryan et al., this volume, for details). This fault strand, which is thought to have left-lateral displacement, clearly shows a history of continuing dip-slip offset with the east side down (Fig. 4B). The core H2 did not penetrate enough of the sandy turbidite sequence to reach even the shallowest offset horizon (yellow in Fig. 4), so even timing of the latest movement cannot be determined. Offset of the seafloor itself is not sufficient because the upper sediment layer could be a drape of hemipelagic sediment of uniform thickness. A nearby core (503) taken on the lower flank of a bathymetric high in San Diego Trough penetrated four meters of sediment, and several of the stronger reflecting horizons could be traced to the fault crossing at core H2 (Figs. 2 and 4A). Radiometric dating of hemipelagic intervals in core 503 shows sediment at the bottom of the core is ca. 40 ka. At the Coronado Bank–Palos Verdes fault crossing, this horizon is offset nearly 1.4 m (Fig. 4B). Ongoing work has shown that this 40 ka horizon can be traced through a grid of seismic-reflection profiles to the Mohole drill site (Figs. 1 and 2) where nearly the same age was determined (Covault et al., 2006; Inman and Goldberg, 1963).

Using the observed fault throw in Figure 4B, the dip-slip component of movement on the Coronado Bank–Palos Verdes fault strand is ~0.35 mm/yr for the past 40 ka. If the fault is dominantly strike-slip, however, it is more difficult to determine the rate of offset. Using the grid of seismic-reflection profiles obtained by the USGS (Fig. 1B), as well as an equally extensive data set acquired from the oil industry (now available at http://walrus.wr.usgs.gov/NAMSS/), it is known that the seafloor in the area of core H2 is sloping gently south (subparallel to the fault trend) at a gradient of 1:500. No multibeam data are available to confirm either this estimate of slope or whether the gently sloping seafloor is approximately planar. For left-lateral displacement along the fault (assuming a planar, gently sloping seafloor) to produce the observed 1.4 m apparent throw would require a strain rate of ~16 mm/yr. This high rate seems unlikely compared with projected strain for other offshore faults in the region (Ryan et al., this volume); thus, without a more accurate measure of the seafloor slope along the fault at the core site, the conservative conclusion is that the motion along the fault probably is a combination of vertical and horizontal offset.

As noted earlier, there were numerous attempts to date displacements on or related to the Palos Verdes fault zone, but this proved more difficult than expected. West of the fault zone on the middle slope south of the San Pedro shelf, sediment on the west side of the main fault trace is gently folded in several anticlinal structures; the section is cut by normal faults, with limited offset, that form flower structures locally (Fisher et al., 2004a, 2004b). One of these normal faults on the upper slope shows offset of ~3.5 m for several prominent reflectors (Fig. 5A). The shallowest offset horizon is less than two meters below the seafloor on the west side of the fault. At this site, a thin sediment cover has smoothed the seafloor and shows no offset. Core 507 was 4 m long, penetrating well below the shallowest offset horizon. The entire core is a mass-wasted deposit mostly matrix-supported, mud-clast conglomerate, with irregular intervals or blebs of sand and silt (facies IIIA of Tripsanas et al., 2008). The firmness and friability of the mud clasts vary throughout the core suggesting a mélange of sediment that had been mobilized from different burial depths but characteristic of failure of surficial material. Three intervals were dated with the youngest age being 24 ka (Fig. 5A). Below the 24 ka sediment is an irregular layer of mud, silty mud, and mud clasts with higher water content than the underlying mud-clast conglomerate, which is ~20 ka older based on two dates. This suggests that there were two episodes of mass failure. The dates are from redeposited material and might not be indicative of the age of the last movement on this strand of the Palos Verdes fault. The alternative interpretation is that the last movement was prior to 24 ka and that the fault was rupturing sedimentary deposits >40 ka. The offset observed in

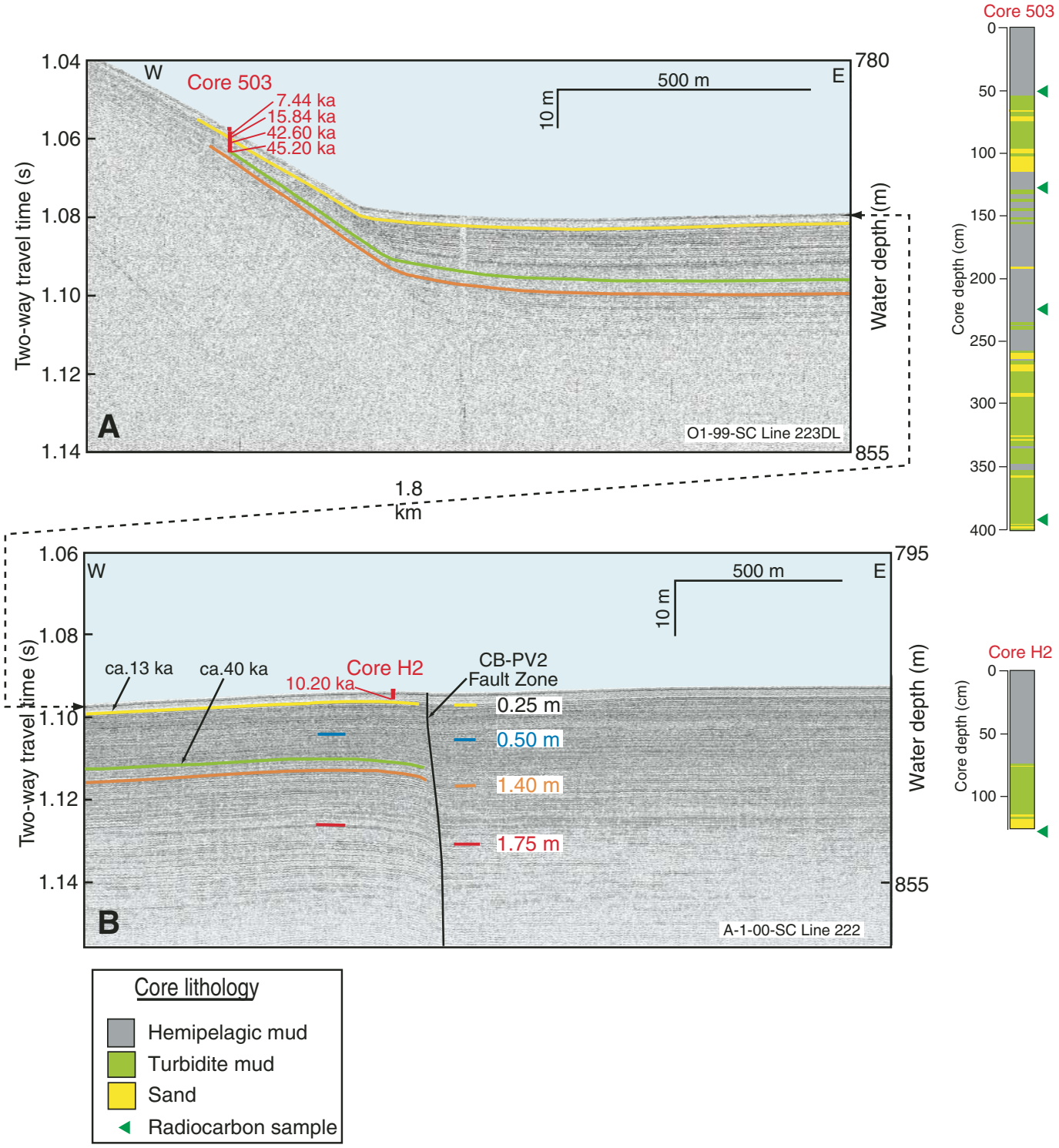

Figure 4. Deep-tow boomer profile segments through cores 503P and H2P together with sediment logs for the cores showing results from (A) dating a condensed section of sediment on the flank of a small bathymetric high and (B) dating a core taken adjacent to the fault to establish the fault offset history. Ages shown are yr B.P. (see Table 6).

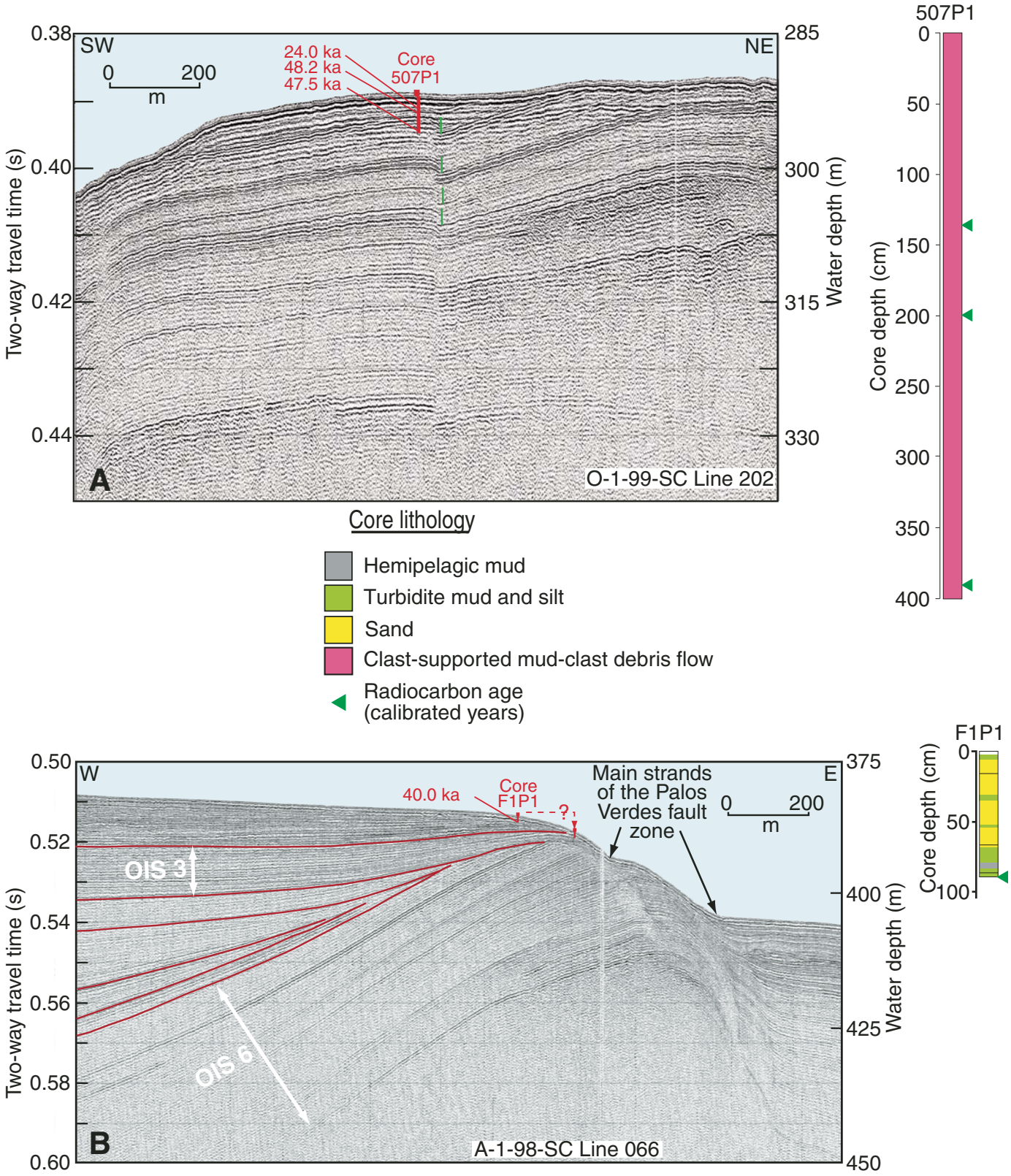

Figure 5. Deep-tow boomer profile segments from the Palos Verdes fault zone together with the sediment logs for two cores taken to date fault activity; see text for explanation. Ages shown are yr B.P. (see Table 4).

the subbottom is probably in late Pleistocene sediment based on interpretation of the record shown in Figure 5B.

The Palos Verdes fault zone is typically associated with marked deformation of the sedimentary units adjacent to the fault, e.g., as seen in a deep-tow boomer profile parallel to and a few kilometers downslope from the profile shown for core Site 507 (Fig. 5A). Similar to the crossing of Coronado Bank–Palos Verdes (Fig. 4B), the fault here shows a long history of deformation in this area of the slope. After truncation and tilting of an ~25 m thick section of well-layered sediment (interval denoted by white arrow in Fig. 5B is tentatively interpreted to be from oxygen isotope stage 6), deformation has continued, resulting in onlap and a series of pinchouts of successive depositional units. The well-bedded acoustic character of the tilted sediment is characteristic of overbank turbidite deposits, which is understandable given that the fault in this locality is just to the west of the channel extending from San Gabriel submarine canyon. It was envisioned that the core from Site F1P1 (Fig. 5B) would recover sediment from the upper part of the youngest tilted sequence, i.e., from near the truncation of the uppermost reflector in the line drawing interpretation. The core was very short, however, having recovered interbedded silty mud and fine sand, the latter being the most common. This turbidite sequence bottoms in sediment nearly 33 ka in age. In this case, the preferred interpretation is that the core probably missed the target site and landed on the fault scarp ~100 m east (probable offset is shown with the dashed line and arrow in Fig. 5B). Continued tilting along the fault post–40 ka does not add to our existing knowledge of the history of movement elsewhere along the Palos Verdes fault (Fisher et al., 2004a, 2004b). If the interpretation of thick overbank sediment deposited during isotope stage 6 is correct, this suggests that much of the tilting of the sequence occurred after 125 ka. Subsequent deposition has ponded behind the area uplifted along the fault and gradually eliminated most of the relief to the west of the fault.

Another site related to the Palos Verdes fault zone is near the summit area of Lasuen Knoll, which is bounded on the west side by the fault. Fisher et al. (2004a) suggest that Lasuen Knoll has been sculpted by erosion at sea level resulting in a series of terraces across the upper 60 m of the summit area. The terrace surfaces, the shallowest of which currently is at 230 m water depth, now tilt three degrees down to the east (Fig. 11 in Fisher et al., 2004a); the tilting is consistent with that observed in sedimentary sections on the east flank of Lasuen Knoll. Core site 504, at 373 m water depth on the northern summit area of Lasuen Knoll, would have been nearly 250 m below sea level during the Last Glacial Maximum (LGM). The core, which consisted mostly of sand and sandy silt beds, recovered a characteristic shelf-edge foraminiferal assemblage without displaced fauna from a thin unit overlying folded and faulted strata. The lower Holocene age of the faunal assemblage in core 504 (Table 4) together with the depth of the summit terraces would suggest that Lasuen Knoll has been sinking since the late Pleistocene.

If submarine slide deposits are shallow enough, it can be relatively easy to establish a time of emplacement using piston-core samples. The Palos Verdes debris avalanche is one of the largest landslides recognized in the inner Borderland (Normark et al., 2004b). Two cores were taken at the same site to establish a date for the slide emplacement. Core 510P2 bottomed in a section of thin-bedded turbidite silt and sand beds dated at ca. 9.3 ka (dashed line in Fig. 6). The high-amplitude reflectors characteristic of the turbidites can be traced under the Palos Verdes debris avalanche on every available deep-tow boomer profile, e.g., Figures 2 and 4 in Normark et al. (2004b), which allowed them to estimate that the avalanche occurred ca. 7.5 ka. It remains unclear, however, whether there were several episodes of failure, e.g., the acoustically transparent interval in the boomer record below one meter depth might be a debris flow deposit generated by a later (than 7.5 ka) slide event.

Larger and more deeply buried submarine slides can be dated, if a deep drill hole is available to provide age control (Lee et al., 2004). The sequence of slides in Santa Barbara Basin has been dated by using seismic-reflection ties to ODP Site 893 (Fisher et al., 2005). The two youngest slides occurred between 8 and 10 ka. The ages of two small, buried slides in southeastern Santa Monica Basin first recognized by Normark and Piper (1998) have now been tied to the dating at ODP 1015. The toes of these small slides are both buried by sediment ca. 9 ka in age. The similarities in age of these failure events in adjacent basins might be explained by seismic shaking during large earthquakes. Lee et al. (this volume) provide a more complete picture of the range of landslide activity in the Borderland.

SEDIMENT-ACCUMULATION RATES

Holocene Accumulation Rates

The radiocarbon dating of the cores from the inner Borderland basins provides an opportunity to evaluate sediment-accumulation rates for the late Quaternary, albeit primarily for the basin floors and landward basin margins. Nearly all piston-core sites penetrated the Holocene or enough of the Holocene to obtain an estimate for average sediment-accumulation rates (Fig. 7). Most of the higher accumulation rates are found in Santa Barbara and Santa Monica Basins, whether the samples are from the basin floor or slope settings. On the Santa Barbara basin slope, rates were between 68 and 174 cm/ka during the past 3 ka compared to rates of 210 cm/ka for the complete Holocene section recovered at nearby ODP Site 893 (24.3 m to base of Holocene; Marsaglia et al., 1995). The highest average Holocene accumulation rate observed was 244 cm/ka at ODP Site 1015 on the floor of Santa Monica Basin. During the Holocene, however, rates at Site 1015 for some intervals exceeded 450 cm/ka (Fig. 7).

Table 7 summarizes the overall Holocene accumulation-rate data for the inner basins with respect to depositional environment, e.g., middle slope, lower slope, basin floor, and interbasin highs. The highest sediment-accumulation rates observed on basin slopes of the inner Borderland is in Santa Barbara Basin;

in contrast, the slopes of the adjacent Santa Monica Basin have rates less than half as much. The highest basin floor rates are observed at ODP Site 1015 indicating the effectiveness of sand-carrying turbidity currents to transport large volumes of sediment through the canyons on the slope of the Santa Clara delta (Fig. 2; Table 7) The accumulation rates on the floor of San Pedro Basin, which is fed by two canyons, and the eastern Gulf of Santa Catalina (Fig. 1), which is fed by the Newport Canyon, are generally less than 50 cm/ka (Table 7). The higher rates for the northern basins (Santa Barbara and Santa Monica) reflect sediment supply from the Transverse Ranges, primarily through the Santa Clara and Ventura Rivers, whose watershed areas provide 75% of the total sediment flux to the Borderland (see Fig. 5 in Warrick and Farnsworth, this volume, Chapter 2.2). Even slower Holocene accumulation rates are observed in the western Gulf of Santa Catalina and San Diego Trough. The lower rate for the former area results from bypassing of much of the sediment from San Gabriel Canyon to Catalina Basin farther west (Normark et al., 2004a). The San Diego Trough is fed primarily by sediment moving in the Oceanside littoral cell (Fig. 2), and this source is cut off as sea level transgresses the shelf (see Normark et al., this volume, Chapter 2.7).

Twelve of the piston cores have three or more radiocarbon dates within the Holocene interval and, together with the eight dates from ODP Site 1015, make it possible to assess changes in accumulation rates as sea level rose after the LGM. Figure 8 illustrates the changes in accumulation rates for Santa Monica Basin and Gulf of Santa Catalina. In Santa Monica Basin, cores SMB1 and SMB2 show rate decreases between 8.2 ka and 1.2 ka and 6.9 ka and 2.6 ka, respectively. SMB1 is from the upper levee of the Dume Fan, and SMB2 is from the lower basin slope west of the Hueneme fan valley (Figs. 2 and 3A). The timing of this decreased supply agrees with the record at ODP 1015 where there is a marked decrease in the interval between 9.4 ka and ca.

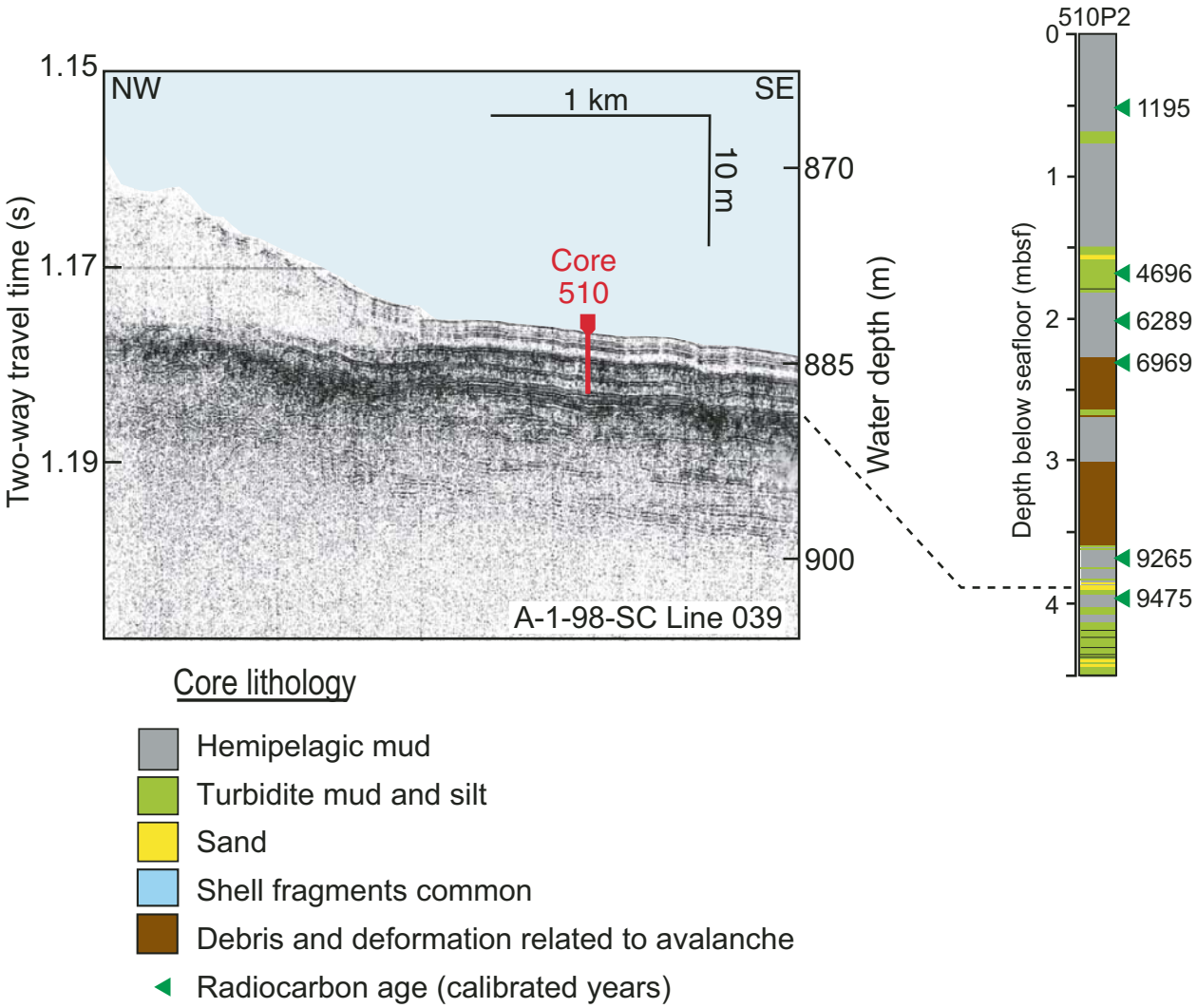

Figure 6. Deep-tow boomer profile segment across the toe of the Palos Verdes debris avalanche together with the sediment log for core 510P2 showing the age of the main avalanche. Ages shown are yr B.P. (see Table 3).

2.2 ka (left sediment log, Fig. 8) followed by a rate increase again after ca. 2.2 ka. The increased sediment-accumulation rate in the late Holocene at least in part results from the progradation of the Santa Clara delta after having been flooded during sea-level rise. Piston core 364 on the lower slope of Santa Monica Basin shows a somewhat similar change, with a decrease after 8.1 ka to 60% of the early Holocene rate (Figs. 8 and 9). The rate does not increase in the late Holocene, but there is an increase in the number of turbidite mud beds reaching the lower slope (Fig. 8).

Core HN2, which is north of and ~300 m water depth shallower than core 364, is near the southern margin of Santa Monica Canyon. The available radiocarbon dates do not show a decrease in middle Holocene accumulation rates but rather suggest a gradual decrease through the Holocene (Fig. 8). This continuing decrease in accumulation rate is consistent with observations of the upper slope and shelf areas of Santa Monica Bay (Sommerfield and Lee, 2003, 2004)

The Newport Canyon system is the primary locus of sediment input for the eastern Gulf of Santa Catalina. Only one of the multiple Newport Canyon heads extends across the shelf during the current highstand, but the system has remained active through the Holocene (Fig. 9 in Dartnell and Gardner, this volume). The multiple heads coalesce downslope, eventually forming a single channel. Core WT1a, which is the most distal sample site for the Newport channel, recovered turbidite sand beds that were deposited within the past 700 yr. Core Site WT1 is on the adjacent channel levee, and the radiocarbon dates document a decreased sediment-accumulation rate between 7.2 and 2.8 ka (Figs. 8 and 9). Core sites from the levee and channel that are more proximal show the same

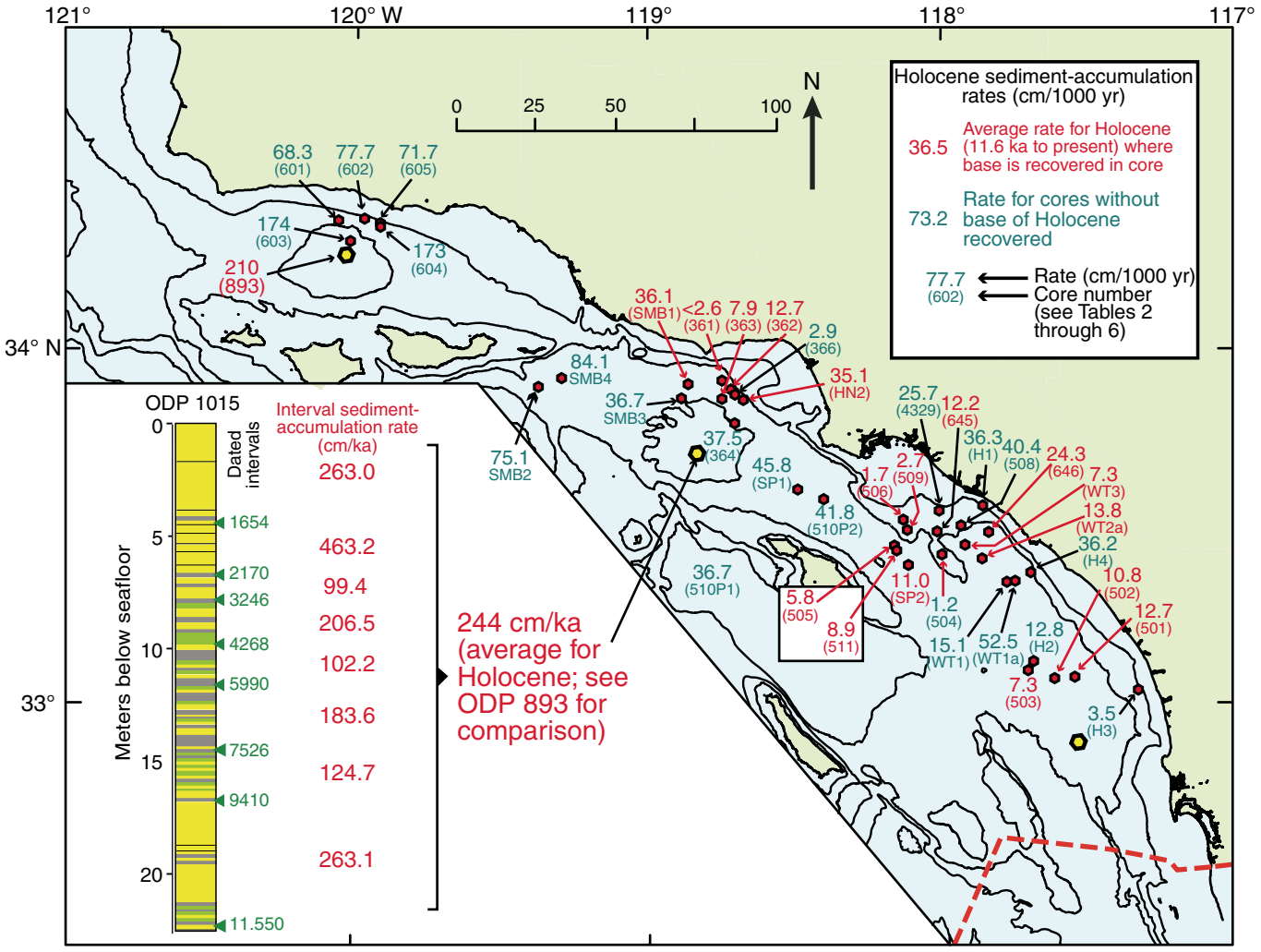

Figure 7. Summary diagram that shows the average Holocene sediment-accumulation rate for the inner basins of the Borderland; the values are in cm/ka with the core designation in parentheses underneath. Refer to Tables 1–6 and Normark and McGann (2004) for full radiocarbon age data. The interpreted depth of the Pleistocene–Holocene boundary where it was recovered is shown by the solid red triangles in core schematics of Figures 2 and 8. The accumulation rates are in red font for cores that penetrated the base of Holocene and in teal, if the core bottomed within the Holocene sequence.

TABLE 7: SEDIMENT-ACCUMULATION RATES VERSUS BASIN BY DEPOSITIONAL ENVIRONMENTS (cm/ka)

Depositional setting	Santa Barbara Basin	Santa Monica Basin	San Pedro Basin	Western Gulf of Santa Catalina	Eastern Gulf of Santa Catalina	San Diego Trough
Middle to upper slope depths	68.3–77.7; lowest rate is on mid slope; higher rates on Goleta slide scar near shelf edge	<2.6–12.7 north of Santa Monica Canyon		1.7–2.7 on slope west of San Gabriel Canyon	25.7–36.3 with higher rate closer to the shelf edge	3.5 on upper slope between La Jolla and Oceanside Fans
Lower slope depths	173.3 on the Goleta slide mass	37.5–75.1; shows turbidity currents are >40 m thick; 40.4 near Santa Monica Canyon			24.3–36.2	
Basin floor including turbidite fans, if present	174.3 on basin floor just off the toe of the Goleta slide mass	Dume Fan: 42.5–36.7 Hueneme Fan: 84.1 (levee) to 244 on basin plain at ODP* Site 1015)	45.8 on sandy lobe of Redondo Fan; 36.7–41.8 south of San Pedro Sea Valley	11.0 on levee of deeply eroded San Gabriel channel	40.4–52.5 in channels from Newport Canyon; 7.3–13.8 on the levees, decreasing downstream	10.8–12.7 on Carlsbad and Oceanside Fans; few turbidite units during Holocene
Ridge and knoll flanks			5.8–8.9 at southeastern corner of basin	1.2 on Lasuen Knoll		7.3 on ridge that partially dams Carlsbad and Oceanside Fan
Turbidite sources	Santa Clara delta	Hueneme, Mugu, Dume, and Santa Monica Canyons	Redondo and San Pedro Sea Valley	San Gabriel Canyon and channel system	Newport Canyon and channel system	Newport, Carlsbad, Oceanside and La Jolla Canyons

*ODP—Ocean Drilling Program.

decreased rate during the middle Holocene. For example, levee core WT2a, which is more proximal (than WT1) on the Newport channel system, shows a marked decrease in rate beginning in the early Holocene but only a modest increase in the past 2.7 ka (Fig. 9). Core 508, which is the most proximal site in the Newport channel system, does not reach the Pleistocene–Holocene boundary. The acoustic character observed in deep-tow boomer profiles suggests that the section cored is dominantly mud. Available dates, however, do show the highest accumulation rate between 2.7 ka and 1.7 ka with lower rates before and after (Figs. 8 and 9).

The increase in sediment-accumulation rates during the late Holocene is best shown in Santa Monica Basin because of the high sediment flux relative to the rest of the Borderland (Warrick and Farnsworth, this volume, Chapter 2.2). The mountainous relief of the Transverse Ranges is adjacent to the coast, and its Tertiary sediments are easily eroded. Sources for the Newport Canyon are farther from the coast and consist of older basement rocks. The limited evidence for increased late Holocene sediment accumulation in both areas might be the result of increased rainfall during this period. Barron et al. (2003) have shown that the El Niño–Southern Oscillation (ENSO) climatic events became enhanced ca. 3.5 ka, thus increasing the frequency of large storms and runoff. In addition, a shift in wave climate ca. 5 ka increased the erosion rate of coastal bluffs (Coastal Morphology Group, 2005).

In the western Gulf of Santa Catalina, core 511 has an acoustic facies typical of overbank turbidites and shows a decrease between 8.6 and 3.4 ka (Figs. 8 and 9). The core is from an uplifted ridge along a fault strand ~10 km west of the primary trace of the Palos Verdes fault zone (Marlow et al., 2000) and probably would be reached only by the largest flows moving through the San Gabriel Canyon system. Similar to the Newport Canyon drainage area, the San Gabriel Canyon is fed by streams arising in the basement rocks of mountains of the same name. A change to a wetter and stormier climate (Barron et al., 2003) is the most likely reason for the observed increased sediment accumulation in the late Holocene.

Comparison of Sediment-Accumulation Rates

In addition to the ODP and Mohole cores, a dozen of the USGS piston cores penetrated enough of the sediment of late Pleistocene age to provide some insight into sediment-accumulation rates during the late Pleistocene. The cartoon of Figure 10 compares the rates for the past 40 ka for three of the inner basins. Basin, lower slope, and middle slope environments are included to the extent possible. Most of the piston cores with multiple radiocarbon dates for oxygen isotope stages (OIS) 2 and 3 are from lower slope areas in basins with lower overall sediment accumulation, hence the cores could penetrate older intervals. Santa Monica Basin has the highest basin-floor accumulation rates as noted earlier, but the mid and upper slope rates during the Holocene in Santa Barbara Basin are the highest

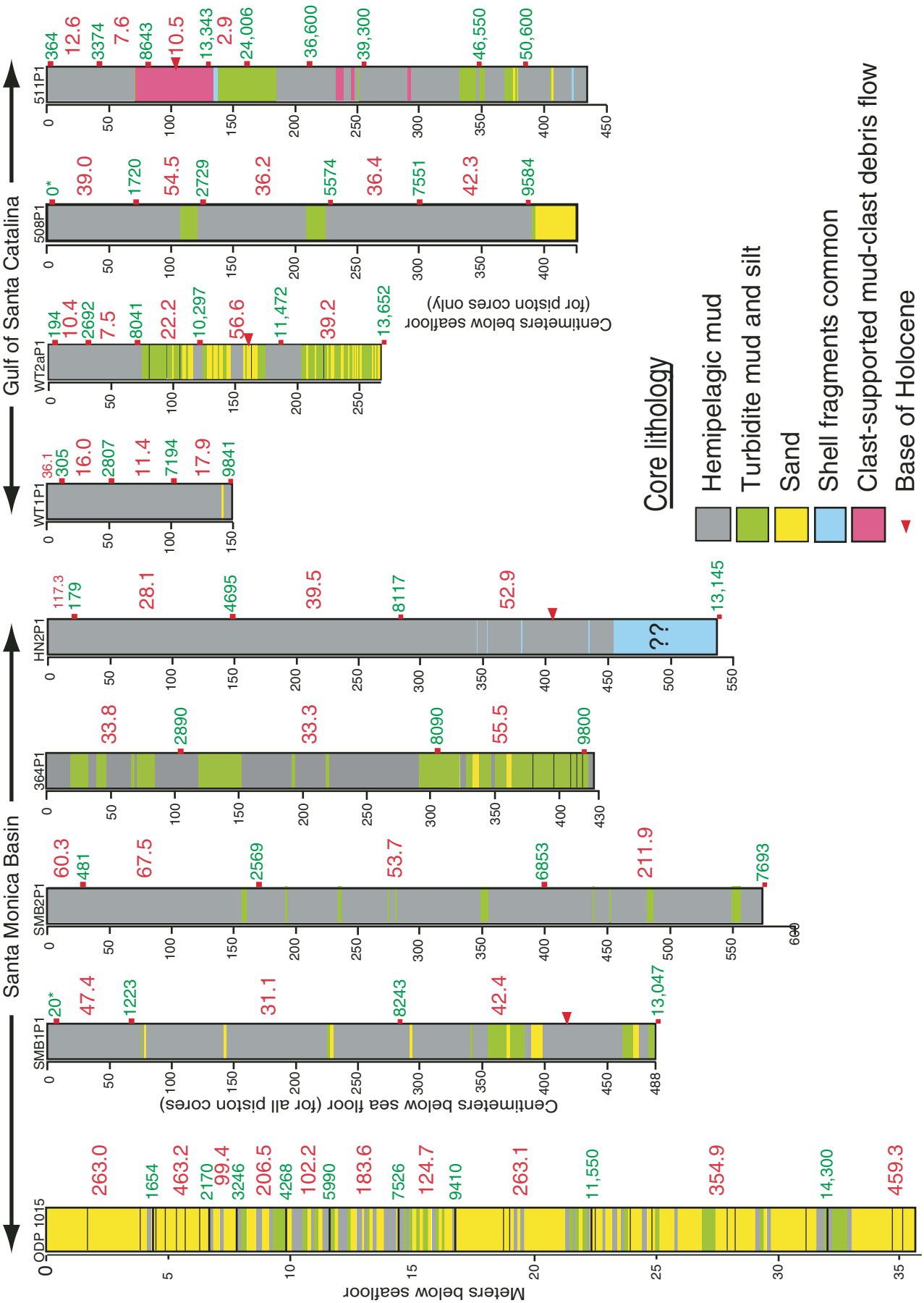

Figure 8. Sediment logs for selected cores from Santa Monica Basin and the Gulf of Santa Catalina to illustrate changes in sedimentation rates during the Holocene: the radiocarbon dates (yr B.P. shown in green) and the sediment-accumulation rate (larger red numbers in cm/ka) between the dated horizons. Refer to Tables 1–6 for full radiocarbon data.

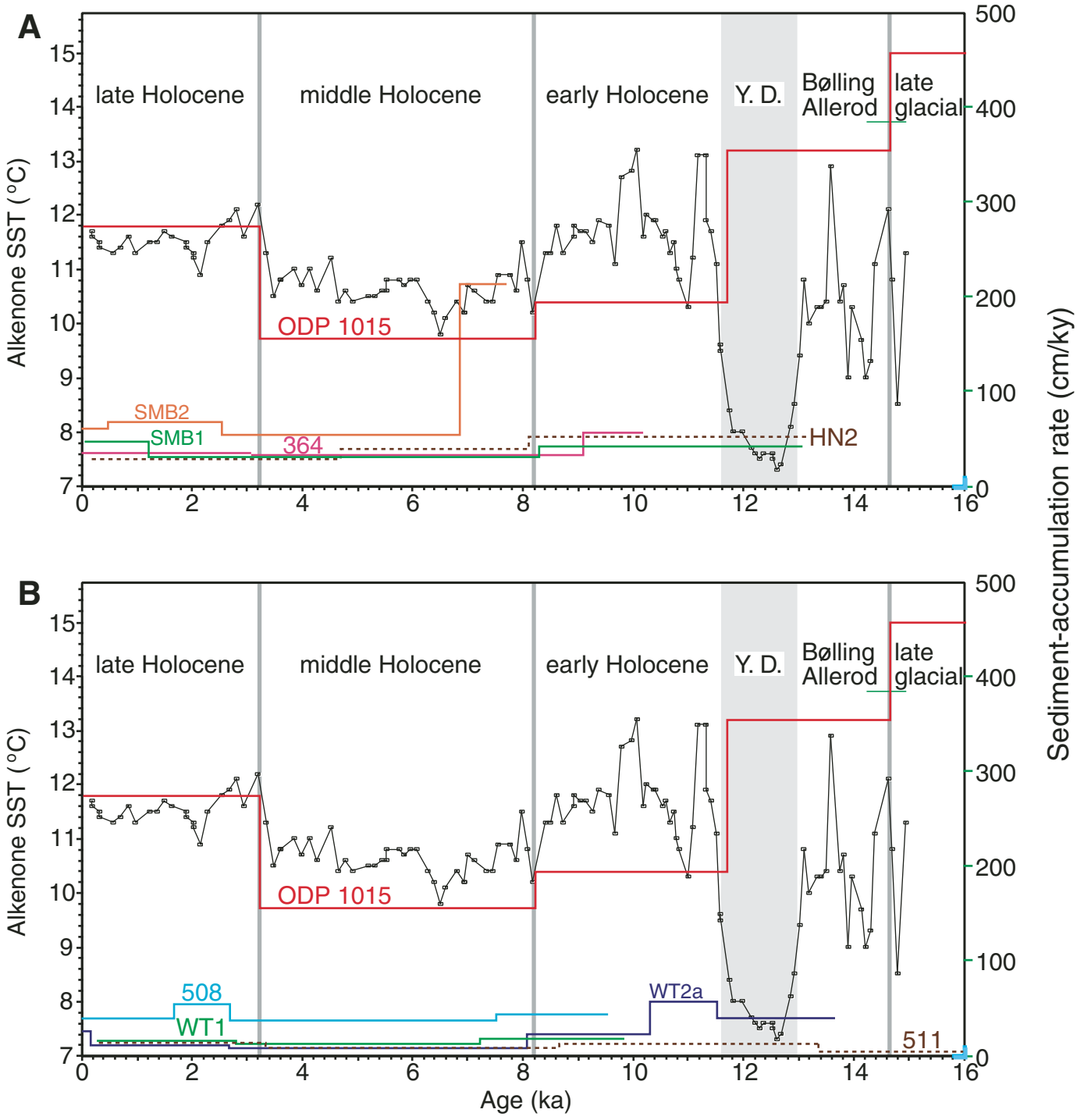

Figure 9. Graphical representation of the sediment-accumulation rates during the past 16 ka for the cores in Figure 8 compared to the alkenone sea-surface temperature (SST) record (black line) for Ocean Drilling Program (ODP) Site 1019 (adapted from Barron et al., 2003). The rates (horizontal line segments) represent the interval between radiocarbon dates. (A) Cores from Santa Monica Basin; (B) cores from the Gulf of Santa Catalina. The rates for ODP Site 1015 are shown in both for comparison. Y.D.—Younger Dryas.

of any of the basins for these environments. This observation is consistent with the relative lack of turbidity-current deposits in the basin compared to Santa Monica Basin. As discussed by Normark et al. (2006), there has been a partitioning of sediment between the two basins for the past 160 ka; much of the fine-grained sediment brought to the Santa Clara delta is moved toward Santa Barbara Basin while the bulk of the sand is transported into Santa Monica Basin. Thus sand comprises 85% of the sediment recovered at ODP Site 1015 (Shipboard Scientific Party, 1997) but less than 10% of the cored interval at ODP Site 893 (Marsaglia et al., 1995).

The Gulf of Santa Catalina shows a marked difference between OIS2 and OIS3 accumulation rates compared with the Holocene (Fig. 10). This difference appears to fit the common perception that most submarine canyons become less active or inactive during high sea-level periods. The core and high-resolution, seismic-reflection data show that both San Gabriel and Newport Canyon systems were active through the Holocene.

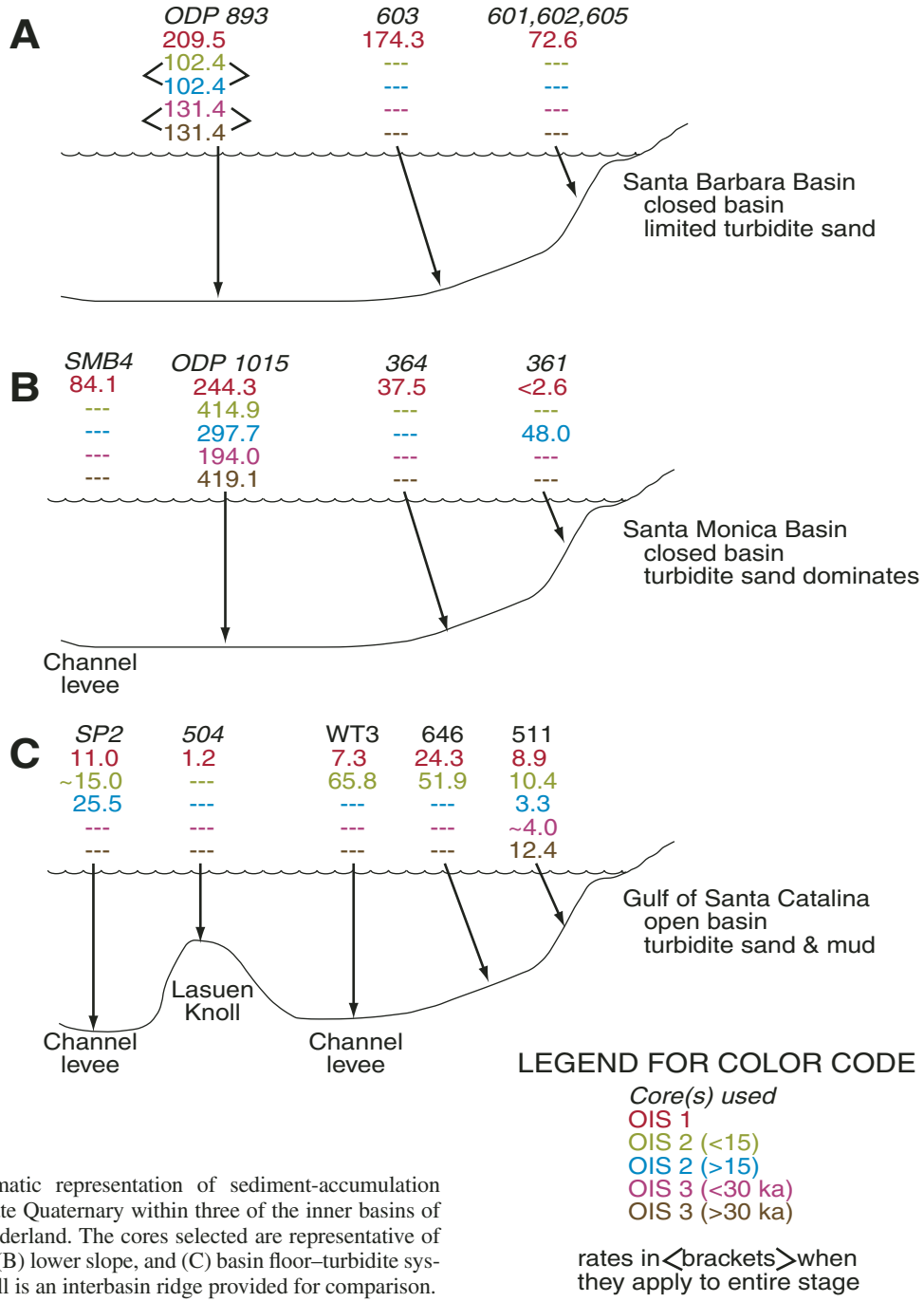

Figure 10. Schematic representation of sediment-accumulation rate data for the late Quaternary within three of the inner basins of the California Borderland. The cores selected are representative of (A) middle slope, (B) lower slope, and (C) basin floor–turbidite systems; Lasuen Knoll is an interbasin ridge provided for comparison.

The size and frequency of the turbidity-current events, however, are reduced, and flows capable of overtopping channel levees are less frequent, e.g., cores SP2, 646, and WT3 (Fig. 10). Cores from intrabasin highs, e.g., 504, show the lowest rates observed.

CONCLUSIONS

Radiocarbon dating of sediment samples from 39 USGS piston cores and from ODP Site 1015 provides time of displacement along faults and emplacement of submarine slides within the inner basins of the California Borderland. Examples of using dated horizons at local sites to evaluate neotectonic activity illustrate the difficulty in using core sites adjacent to fault traces to determine offset histories, primarily because of the relatively sandy nature of the sediment deposited in the inner basins of the Borderland. Dating condensed sections on slopes adjacent to fault zones provides better control on fault history where high-resolution, seismic-reflection data can be used to correlate sediment between the core site and the fault zones. Where possible, establishing a more regional, high-resolution, chronostratigraphic framework is preferable for neotectonic interpretation of both fault strain and landslide failures.

The USGS core sites were selected to support the geologic hazard activity (see also Section 4), but are used herein to examine sediment-accumulation rates in the basins. As expected, the dating confirms a decrease at most sites in accumulation rates during sea-level rise from the LGM. Basins fed directly by rivers, however, show an increase in sediment-accumulation rates in the late Holocene, well after sea level reached the current highstand position. Locally, river deltas were able to advance sufficiently to maintain contact with submarine canyons (e.g., Santa Clara delta leading to western Santa Monica Basin) or the feeding canyons were able to maintain their heads near the river mouths (Newport Canyon in the Gulf of Santa Catalina). In addition, there was increased sediment supply to the basins as a result of an increased frequency of ENSO events at 3.5 ka and increased coastal erosion at 5 ka (Barron et al., 2003; Coastal Morphology Group, 2005). The most marked change in sediment-accumulation rates occurs within basins fed by sediment moving in littoral cells; in these cases, the data show that while some canyons may lose their source of sediment, e.g., Santa Monica Canyon, other canyons in the area can benefit, e.g., Redondo Canyon feeding San Pedro Basin (see also Normark et al., this volume, Chapter 2.7).

ACKNOWLEDGMENTS

The authors thank scientific parties and ship's crew on cruises A-2-98-SC, O-2-99-SC, and A-1-02-SC for obtaining the piston cores used for this study. We also recognize C.E. Gutmacher and R. Keaten for their assistance, respectively, in providing base bathymetric maps and assisting with core descriptions. The manuscript benefited by critical reviews from H. Gibbons, J.A. Barron, and D.J.W. Piper.

REFERENCES CITED

Alexander, C.R., and Lee, H.J., 2009, this volume, Sediment accumulation on the Southern California Bight continental margin during the twentieth century, *in* Lee, H.J., and Normark, W.R., eds., Earth Science in the Urban Ocean: The Southern California Continental Borderland: Geological Society of America Special Paper 454, doi: 10.1130/2009.2454(2.4).

Barron, J.A., Heusser, L., Herbert, T., and Lyle, M., 2003, High-resolution climatic evolution of coastal northern California during the past 16,000 years: Paleoceanography, v. 18, 10.1029/2002PA000768,

Behl, R., and Kennett, J.P., 1996, Brief interstadial events in the Santa Barbara basin, NE Pacific, during the past 60 kyr: Nature, v. 379, p. 243–246.

Behl, R.J., Kennett, J.P., Hill, T.M., Pak, D., Schimmelmann, A., Cannariato, K.G., Nicholson, C., Hopkins, S.E., Team, S., 2005, Extending the high-resolution global climate record in Santa Barbara Basin: Developing a more continuous composite section from overlapping Cores: Eos (Transactions, American Geophysical Union), v. 86, no. 52, Fall Meeting Supplement, Abstract PP51D-0636.

Christensen, C.J., Gorsline, D.S., Hammond, D.W., and Lund, S.P., 1994, Non-annual laminations and expansion of anoxic basin floor conditions in Santa Monica Basin, California Borderland, over the past four centuries: Marine Geology, v. 116, p. 399–418, doi: 10.1016/0025-3227(94)90054-X.

Coastal Morphology Group, 2005, Living with coastal change then and now: Scripps Institution of Oceanography, http://coastalchange.ucsd.edu/st1_thenandnow/.

Covault, J.A., Normark, W.R., and Graham, S.A., 2006, Source to sink continuity through relative sea-level changes from OIS 3 to the present: Only the pathway changes in the California Borderland: Eos (Transactions, American Geophysical Union), v. 87, no. 52, Fall Meeting Suppl., Abstract OS23A-1632.

Dartnell, P., and Gardner, J.V., 2009, this volume, Seafloor terrain analysis and geomorphology of the greater Los Angeles margin and San Pedro Basin, Southern California, *in* Lee, H.J., and Normark, W.R., eds., Earth Science in the Urban Ocean: The Southern California Continental Borderland: Geological Society of America Special Paper 454, doi: 10.1130/2009.2454(1.2).

Fisher, M.A., Normark, W.R., Bohannon, R.G., Sliter, R.W., and Calvert, A.J., 2003, Geology of the continental margin beneath Santa Monica Bay, Southern California, from seismic-reflection data: Bulletin of the Seismological Society of America, v. 93, p. 1955–1983, doi: 10.1785/0120020019.

Fisher, M.A., Normark, W.R., Langenheim, V.E., Calvert, A.J., and Sliter, R., 2004a, Marine geology and earthquake hazards of the San Pedro shelf region, southern California: U.S. Geological Survey Professional Paper 1687, http://geopubs.wr.usgs.gov/.

Fisher, M.A., Normark, W.R., Langenheim, V.E., Calvert, A.J., and Sliter, R., 2004b, The offshore Palos Verdes Fault Zone near San Pedro, southern California: Bulletin of the Seismological Society of America, v. 94, p. 506–530, doi: 10.1785/0120030042.

Fisher, M.A., Normark, W.R., and Greene, H.G., Lee, H.J., and Sliter, R.W., 2005, Geology and tsunamigenic potential of submarine landslides in Santa Barbara Channel, Southern California: Marine Geology, v. 224, p. 1–22.

Fisher, M.A., Sorlien, C.C., and Sliter, R.W., 2009, this volume, Potential earthquake faults offshore Southern California, from the eastern Santa Barbara Channel south to Dana Point, *in* Lee, H.J., and Normark, W.R., eds., Earth Science in the Urban Ocean: The Southern California Continental Borderland: Geological Society of America Special Paper 454, doi: 10.1130/2009.2454(4.4).

Gorsline, D.S., 1996, Depositional events in Santa Monica Basin, California Borderland, over the past five centuries: Sedimentary Geology, v. 104, p. 73–88, doi: 10.1016/0037-0738(95)00121-2.

Gorsline, D.S., and Emery, K.O., 1959, Turbidity current deposits in San Pedro and Santa Monica Basins off southern California: Geological Society of America Bulletin v. 70, p. 279–290, doi: 10.1130/0016-7606(1959)70[279:TDISPA]2.0.CO;2.

Greene, H.G., Murai, L.Y., Ward, S.N., Fisher, M.A., Paull, C.E., Lee, H.J., Normark, W.R., and Maher, N.A., 2004, Types and mechanisms of mass-wasting events that shape the California continental margin, USA: 57th Canadian Geotechnical Conference, October 2004, G36554 pdf, p. 1–7.

Gutmacher, C.E., Normark, W.R., Ross, S.L., Edwards, B.D., Sliter, R., Hart, P., Cooper, B., Childs, J., and Reid, J.A., 2000, Cruise report for A1-00-SC Southern California earthquake hazards project, Part A: U.S. Geological Survey Open-File Report 00-516, 67 p.

Inman, D.L., and Goldberg, E.D., 1963, Petrogenesis and depositional rates of sediments from the experimental Mohole drilling off La Jolla, California: Eos (Transactions, American Geophysical Union), v. 44, p. 68.

Kennett, J.P., and Venz, K., 1995, Late Quaternary climatically related planktonic foraminiferal assemblage changes: Hole 893A, Santa Barbara Basin, California, *in* Kennett, J.P., Baldauf, J.G., and Lyle, M., eds., Proceedings of the Ocean Drilling Program, Scientific Results: College Station, Texas, Ocean Drilling Program, v. 146, no. 2, p. 281–293.

Kennett, J.P., Kennett, J.P., Behl, R.J., Hill, T., Pak, D., Schimmelmann, A., Cannariato, K., Nicholson, C., Sorlien, C.C., and Hopkins, S.E., 2005, Extending the high-resolution global climate record in Santa Barbara Basin: Preliminary results and implications: Eos (Transactions, American Geophysical Union) v. 86, no. 52, Fall Meeting Supplement, Abstract PP34B-02.

Kienast, S.S., and McKay, J.L., 2001, Sea surface temperatures in the subarctic northeast Pacific reflect millennial-scale climate oscillations during the last 16 kyrs: Geophysical Research Letters, v. 28, p. 1563–1566, doi: 10.1029/2000GL012543.

Kovanen, D.J., and Easterbrook, D.J., 2002, Paleodeviations of radiocarbon marine reservoir values for the northeast Pacific: Geology, v. 30, p. 243–246, doi: 10.1130/0091-7613(2002)030<0243:PORMRV>2.0.CO;2.

Lee, H.J., Normark, W.R., Fisher, M.A., Greene, H.G., Edwards, B.D., and Locat, J., 2004, Timing and extent of submarine landslides in Southern California: Offshore Technology Conference 2004, OTC Paper No. 16744, 12 p.

Lee, H.J., Greene, H.G., Edwards, B., Fisher, M.A., and Normark, W.R., 2009, this volume, Submarine landslides of the Southern California Borderland, *in* Lee, H.J., and Normark, W.R., eds., Earth Science in the Urban Ocean: The Southern California Continental Borderland: Geological Society of America Special Paper 454, doi: 10.1130/2009.2454(4.3).

Marlow, M.S., Gardner, J.V., and Normark, W.R., 2000, Using high-resolution multibeam bathymetry to identify seafloor surface rupture along the Palos Verdes fault complex in offshore southern California: Geology, v. 28, p. 587–590, doi: 10.1130/0091-7613(2000)28<587:UHMBTI>2.0.CO;2.

Marsaglia, K.M., Rimkus, K.C., and Behl, R.J., 1995, Provenance of sand deposited in the Santa Barbara Basin at Site 893 during the last 155,000 years, *in* Kennett, J.P., Baldauf, J.G., and Lyle, M., eds., Proceedings of the Ocean Drilling Program, Scientific Results: College Station, Texas, Ocean Drilling Program, v. 146, no. 2, p. 61–75.

Martinson, D.G., Pisias, N.G., Hays, J.D., Imbrie, J., Moore, T.C., Jr., and Shackleton, N.J., 1987, Age dating and the orbital theory of the ice ages: Development of a high-resolution 0 to 300,000-year chronostratigraphy: Quaternary Research, v. 27, p. 1–29, doi: 10.1016/0033-5894(87)90046-9.

Mix, A.C., Lund, D.C., Pisias, N.G., and Bodén, P., 1999, Rapid climate oscillations in the northeast Pacific during the last deglaciation reflect Northern and Southern Hemisphere sources, *in* Clark, P., Webb, R.S., and Keigwin, L.D., eds., Mechanisms for global climate change at millennial time scales: Washington, D.C., American Geophysical Union, Geophysical Monograph Series, v. 112, p. 127–148.

Nardin, T.R., 1983, Late Quaternary depositional systems and sea level change—Santa Monica and San Pedro Basins, California Continental Borderland: American Association of Petroleum Geologists Bulletin, v. 67, p. 1104–1124.

National Oceanic and Atmospheric Administration (NOAA), 1998, NOS hydrographic survey data, U.S. coastal waters: Boulder, Colorado, World Data Center for Marine Geology and Geophysics, Data Announcement 01-MGG-03. (Data available at: http://www.ngdc.noaa.gov/mgg/fliers/01mgg03.html).

Normark, W.R., and McGann, M., 2004, Late Quaternary deposition in the inner basins of the California continental borderland—Part A. Santa Monica Basin: U.S. Geological Survey Scientific Investigations Report 2004-5183, 21 p.

Normark, W.R., and Piper, D.J.W., 1998, Preliminary evaluation of recent movement on structures within the Santa Monica Basin, offshore southern California: U.S. Geological Survey Open-File Report 98-518, 60 p.

Normark, W.R., Piper, D.J.W., and Hiscott, R.N., 1998, Sea level effects on the depositional architecture of the Hueneme and associated submarine fan systems, Santa Monica Basin, California: Sedimentology, v. 45, p. 53–70, doi: 10.1046/j.1365-3091.1998.00139.x.

Normark, W.R., Piper, D.J.W., and Sliter, R., 2006, Sea-level and tectonic control of middle to late Pleistocene turbidite systems in Santa Monica Basin, offshore California: Sedimentology, v. 53, p. 867–897, doi: 10.1111/j.1365-3091.2006.00797.x.

Normark, W.R., Bohannon, R.G., Sliter, R., Dunhill, G., Scholl, D.W., Laursen, J., Reid, J.A., and Holton, D., 1999a, Cruise report for A1-98-SC Southern California earthquake hazards project: U.S. Geological Survey Open-File Report 99-152, 60 p.

Normark, W.R., Reid, J.A., Sliter, R.W., Holton, D.J., Gutmacher, C.E., Fisher, M.A., and Childs, J.C., 1999b, Cruise report for O1-99-SC Southern California earthquake hazards project: U.S. Geological Survey Open-File Report 99-560, 60 p.

Normark, W.R., Fisher, M.A., Gutmacher, C.E., Sliter, R., Hibbeler, L., Feingold, B., and Reid, J.A., 2003, Cruise report for A1-02-SC Southern California CABRILLO project, Earthquake Hazards Task: U.S. Geological Survey Open-File Report 03-110, 68 p.

Normark, W.R., Baher, S., and Sliter, R., 2004a, Late Quaternary sedimentation and deformation in Santa Monica and Catalina Basins, offshore southern California, *in* Legg, M., Davis, P., and Gath, E., eds., Geology and tectonics of Santa Catalina Island and the California Continental Borderland: Santa Ana, South Coast Geological Society Annual Field Trip Guidebook, p. 291–317.

Normark, W.R., McGann, M., and Sliter, R., 2004b, Age of Palos Verdes submarine debris avalanche, southern California: Marine Geology, v. 203, p. 247–259, doi: 10.1016/S0025-3227(03)00308-6.

Normark, W.R., Piper, D.J.W., Romans, B.W., Covault, J.A., Dartnell, P., and Sliter, R.W., 2009, this volume, Submarine canyon and fan systems of the California Continental Borderland, *in* Lee, H.J., and Normark, W.R., eds., Earth Science in the Urban Ocean: The Southern California Continental Borderland: Geological Society of America Special Paper 454, doi: 10.1130/2009.2454(2.7).

Piper, D.J.W., Hiscott, R.N., and Normark, W.R., 1999, Outcrop-scale acoustic facies analysis and latest Quaternary development of Hueneme and Dume submarine fans, offshore California: Sedimentology, v. 46, p. 47–78, doi: 10.1046/j.1365-3091.1999.00203.x.

Reynolds, S., 1987, A recent turbidity current event, Hueneme fan, California: Reconstruction of flow properties: Sedimentology, v. 34, p. 129–137, doi: 10.1111/j.1365-3091.1987.tb00565.x.

Ryan, H.F., Legg, M.R., Conrad, J.E., and Sliter, R.W., 2009, this volume, Recent faulting in the Gulf of Santa Catalina: San Diego to Dana Point, *in* Lee, H.J., and Normark, W.R., eds., Earth Science in the Urban Ocean: The Southern California Continental Borderland: Geological Society of America Special Paper 454, doi: 10.1130/2009.2454(4.5).

Shackleton, N.J., Fairbanks, R.G., Tzu-chien Chiub, and Parreninc, F., 2004, Absolute calibration of the Greenland time scale: Implications for Antarctic time scales and for $\Delta^{14}C$: Quaternary Science Reviews Rapid Communication, v. 23, p. 1513–1522.

Shipboard Scientific Party, 1997, Site 1015, *in* Lyle, M., Koizumi, I., Richter, C., et al.., Proceedings of the Ocean Drilling Program: College Station, Texas, Ocean Drilling Program, Initial Reports, 167, p. 223–237.

Shorebased Scientific Party, 1994, Site 893, *in* Kennett, J.P., Baldauf, J., et al., Proceedings of the Ocean Drilling Program: College Station, Texas, Ocean Drilling Program, Initial Reports, 146, pt. 2, p. 15–50.

Sommerfield, C.K., and Lee, H.J., 2003, Magnitude and variability of Holocene sediment accumulation in Santa Monica Bay, California: Marine Environmental Research, v. 56, no. 1–2, p. 151–176, doi: 10.1016/S0141-1136(02)00329-X.

Sommerfield, C.K., and Lee, H.J., 2004, Across-shelf sediment transport since the last glacial maximum, Southern California margin: Geology, v. 32, no. 4, p. 345–348, doi: 10.1130/G20182.2.

Sommerfield, C.K., Lee, H.J., and Normark, W.R., 2009, this volume, Postglacial sedimentary record of the Southern California continental shelf and slope, Point Conception to Dana Point, *in* Lee, H.J., and Normark, W.R., eds., Earth Science in the Urban Ocean: The Southern California Continental Borderland: Geological Society of America Special Paper 454, doi: 10.1130/2009.2454(2.5).

Southon, J.R., Nelson, D.E., and Vogel, J.S., 1990, A record of past ocean-atmosphere radiocarbon differences from the Northeast Pacific: Paleoceanography, v. 5, p. 197–206, doi: 10.1029/PA005i002p00197.

Stuiver, M., and Polach, H.A., 1977, Discussion: Reporting of ^{14}C data: Radiocarbon, v. 19, p. 355–363.

Stuiver, M., and Reimer, P.J., 1993, Extended ^{14}C database and revised CALIB radiocarbon calibration program (version 5.0): Radiocarbon, v. 35, p. 215–230.

Tripsanas, E., Piper, D.J.W., Jenner, K.A., and Bryant, W.R., 2008, Sedimentary characteristics of submarine mass-transport deposits: New perspectives from a core-based facies classification: Sedimentology, v. 55, p. 97–136.

Warrick, J.A., and Farnsworth, K.L., 2009, this volume, Sources of sediment to the coastal waters of the Southern California Bight, *in* Lee, H.J., and Normark, W.R., eds., Earth Science in the Urban Ocean: The Southern California Continental Borderland: Geological Society of America Special Paper 454, doi: 10.1130/2009.2454(2.2).

Manuscript Accepted by the Society 5 November 2008

Printed in the USA